ACS NANO

www.acsnano.org

PERSPECTIVE

Integrative Approaches to Reveal Catalyst Dynamics: Bridging *Operando* Techniques, Theory, and Artificial Intelligence

Tae Hyung Lee,[†] Serin Lee,[†] Lin Yuan, Jennifer A. Dionne,* and Jungwon Park*

Cite This: https://doi.org/10.1021/acsnano.5c10976 Read Online

ACCESS | Metrics & More | Article Recommendations

ABSTRACT: **Catalysts operate under complex conditions that require sophisticated approaches to understand their dynamics. This perspective outlines advances in experimental *operando* techniques, theoretical approaches, and machine learning (ML)-based data analysis to elucidate catalyst dynamics and improve the next-generation catalyst design. We first survey *operando* techniques, spanning electron microscopy, X-ray spectroscopy, and vibrational spectroscopy, that capture catalyst dynamics under operating conditions. We then discuss how *operando* observations integrate with and inform theoretical models, creating an iterative feedback loop between experiment and computation. Finally, we highlight how advanced data analysis, especially ML, enables the interpretation of high-dimensional *operando* data sets and can even inform catalyst design. Together, these synergetic approaches provide a unified framework for probing catalyst function and accelerating the rational design of efficient, durable catalytic systems for sustainable chemical manufacturing.**

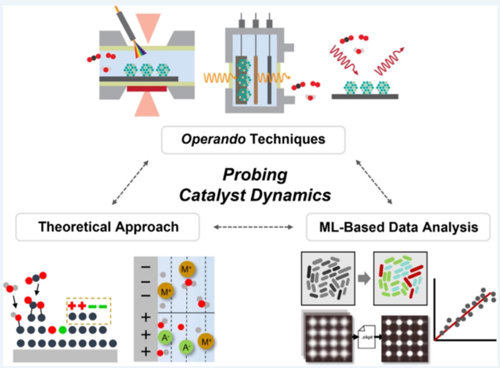

KEYWORDS: *operando techniques, catalyst dynamics, machine learning, theory−experiment integration, rational catalyst design*

INTRODUCTION

Today's chemical industry contributes to over 24% of global greenhouse gas emissions due to its reliance on heat-intensive thermochemical processes.[1] To enable more sustainable chemical manufacturing, much progress has been made in the design of electro-, photo-, and biocatalysts, which can operate under lower temperature and pressure conditions. Still, optimizing catalysts for sustainable industrial manufacturing will require an improved understanding of how the atomic-scale structure impacts function. During catalytic reactions, catalysts undergo multifaceted physical, chemical, and structural changes. These changes not only affect the lifetime of the catalyst but also modulate reaction pathways, thereby impacting performance.[2] These changes are termed "catalyst dynamics"; they reflect the evolving nature of the active sites that can either enhance or degrade the overall catalytic performance, including the activity, rate, and selectivity.[3] There is considerable value in studying these dynamics under realistic operating conditions to improve efficiency and innovation in catalytic technology.

Recent advances in *in situ* techniques have enabled the capture and explanation of the dynamic behavior of catalysts.[4] The term "*in situ*" derives from the Latin phrase meaning "in place". It refers to the real-time recording of catalyst dynamics while simulating one or some of the reaction conditions by coupling with controlled external stimuli.[5,6] However, a stark contrast often exists between operating conditions in industrial catalytic reactors and those that can be achieved in traditional *in situ* measurements. Common industrial reactions, such as the Haber−Bosch process for ammonia synthesis, occur at extreme pressures (150−350 bar),[7] while propane dehydrogenation operates at elevated temperatures of 550−750 °C.[8] Similarly, processes like steam methane reforming for blue hydrogen production demand even harsher conditions, typically ranging from 700 to 1000 °C and pressures of 3−35 bar.[9] In the realm of electrocatalysis, processes such as the oxygen evolution reaction involve complex liquid phases and electrochemical biases.[10] Likewise, photocatalysis requires

Received: July 1, 2025
Revised: October 9, 2025
Accepted: October 9, 2025

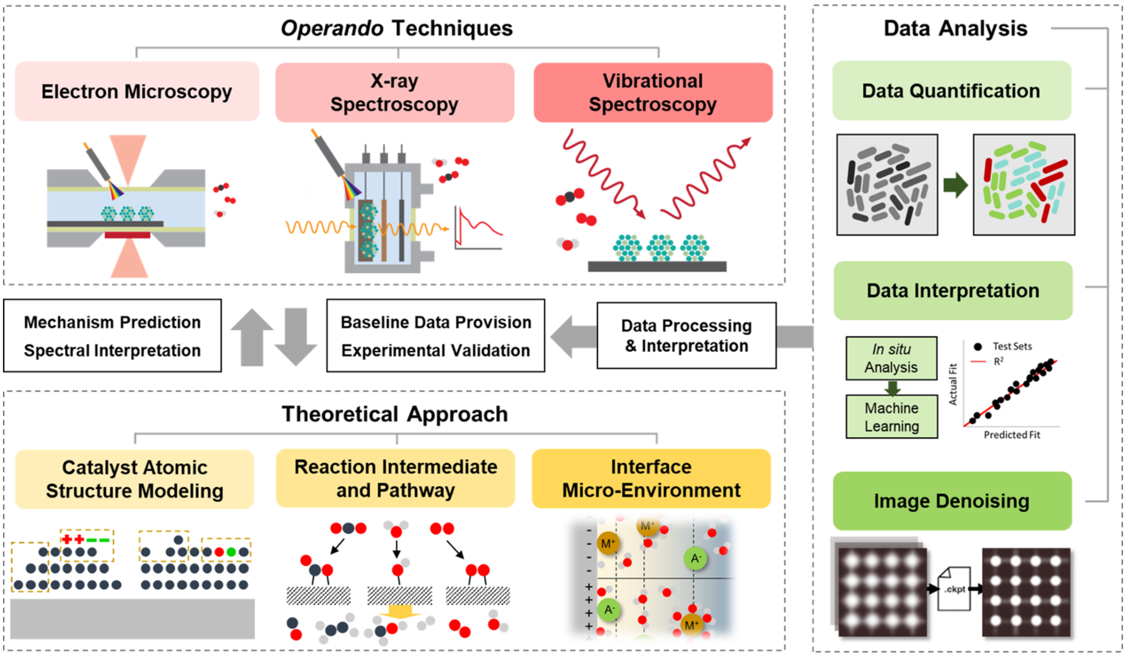

Figure 1. Complementary feedback cycle between *operando* techniques, theoretical approach, and data analysis of catalyst dynamics.

controlled conditions of light illumination to replicate real-world operating conditions such as those found in nature (e.g., to understand photosynthesis or nitrogen fixation)[11] or to design next-generation light-driven industrial photoreactors.[12] How can one obtain dynamic structure−property−performance relations while operating under reactive gaseous or liquid environments and with varying temperatures, pressures, and electrical and optical biases? To answer this question, a significant amount of effort has been recently made to transition *in situ* techniques toward *operando* measurements.

"*Operando*" measurements use *in situ* techniques to simultaneously measure physical/chemical phenomena and system performance during catalytic operation.[13] In particular, *operando* measurements emphasize achieving multiple experimental conditions to fully simulate working or operating conditions, capturing a more realistic picture of the catalytic process.[5,6,13−17] Achieving realistic *operando* conditions involves not only monitoring catalysts during operation but also ensuring that these conditions replicate the industrial or environmental parameters in which the catalysts will be used. These operating conditions are usually achieved by engineering the environment implemented in the platform for *in situ* measurements, such as by connecting with microfluidic channels for introducing liquid, exposing the sample to the gas through differential pumping, applying electrochemical biasing, and controlling temperature. Yet, due to the inherently confined nature of most equipment for *operando* measurements, the environments implemented in *operando* experiments lack the complexity of the bulk operating conditions.[18] Therefore, a comprehensive understanding of catalyst dynamics can only be achieved through the cross-validation between multiple complementary *operando* techniques. However, integrating insights from multiple techniques introduces new challenges in interpretation. The diverse nature of *operando* data, ranging in spatial and temporal resolution, signal type, and sensitivity to different catalytic properties, necessitates a rigorous framework for correlation and validation. This is where theoretical modeling becomes essential. Theoretical approaches, such as density functional theory (DFT) and molecular dynamics (MD) can help contextualize experimental observations, clarify underlying mechanisms, and guide the selection of relevant experimental parameters. Conversely, *operando* data provide critical benchmarks for refining theoretical models, improving their accuracy, and predictive power. Yet, the increasing volume and complexity of *operando* data also call for advanced data analysis strategies. As these data sets grow in both size and dimensionality, traditional manual interpretation becomes insufficient. Emerging machine learning (ML) algorithms offer powerful capabilities to extract patterns, classify dynamic behaviors, and even predict catalytic performance based on multidimensional data streams.

In this perspective, we highlight strategies that leverage the synergy between *operando* techniques, theoretical modeling, and data-driven analysis to uncover the complex dynamics of catalytic systems. We begin by surveying key *operando* techniques, such as electron microscopy (EM), X-ray spectroscopy, and vibrational spectroscopy, that offer distinct yet complementary views of catalyst behavior under working conditions. When combined, these techniques can bridge the gap between simplified *operando* models and real-world catalytic environments. Next, we examine how *operando* data fit into the iterative feedback loop between experiment and theory. Real-time observations serve both to validate and refine theoretical models, including those based on DFT, while theoretical predictions help interpret experimental signals and guide future measurements. Finally, we explore advanced data analysis approaches designed to manage the volume and complexity of *operando* data sets. Here, AI, particularly ML, plays a pivotal role in uncovering trends, identifying reaction patterns, and predicting catalytic outcomes from high-dimensional, time-resolved data. By integrating these three pillars, *operando* experimentation, theory, and ML-based data analysis, we propose a unified framework to more effectively capture and understand catalyst dynamics, ultimately driving the design of more efficient and robust catalytic systems (Figure 1).

https://doi.org/10.1021/acsnano.5c10976
ACS Nano XXXX, XXX, XXX−XXX

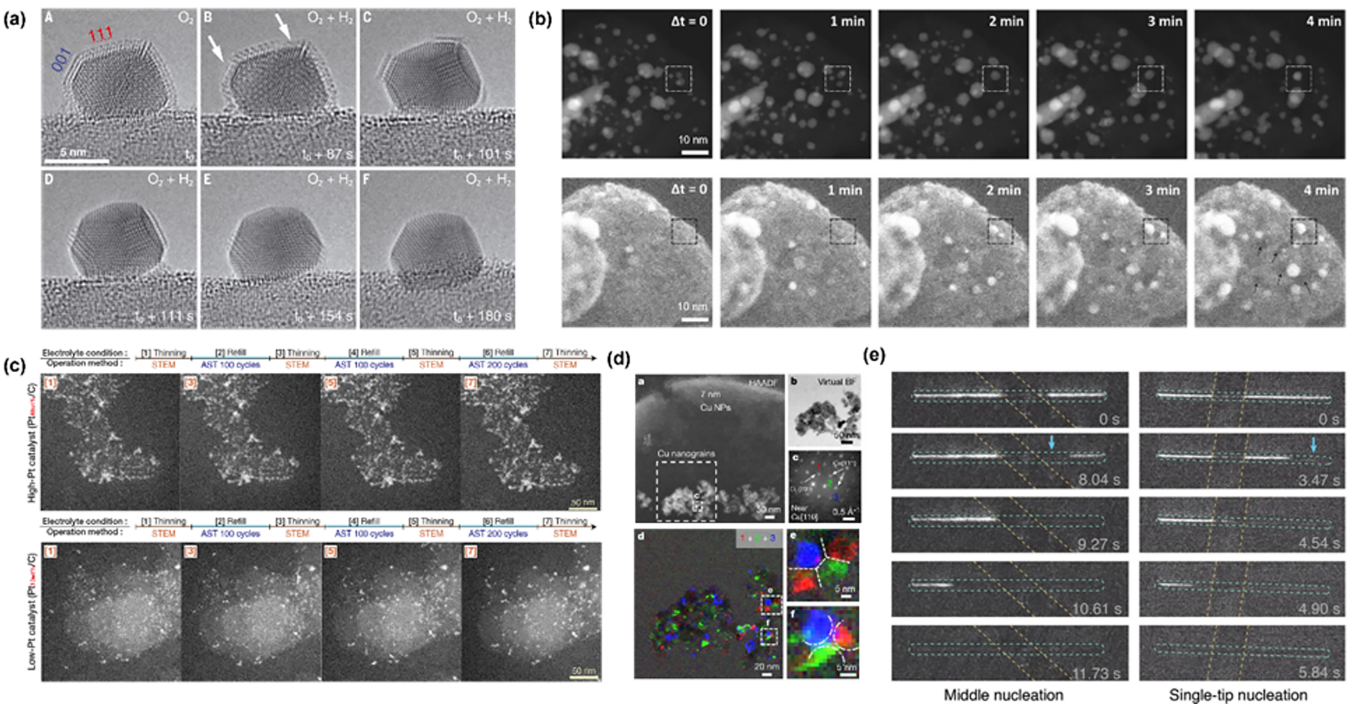

Figure 2. Characterization of catalyst dynamics under controlled environmental conditions followed by multimodal outputs through *operando* electron microscopy. (a) Pt nanoparticle dynamics under redox conditions in a gas environment. (b) Sintering and degradation of support observed via HAADF-STEM (top) and SE (bottom) imaging. (c) Degradation of the electrocatalyst with high Pt (top) and low Pt (bottom) loading on a carbon support, during electrochemical cycling under accelerated stress test (ACT) conditions in a liquid environment. (d) Morphology evolution of Cu catalyst during electrochemical CO2RR captured through 4D-STEM. (e) Light-driven H_2 absorption of Pd captured through optically coupled TEM. Adapted with permission from ref 81. Copyright 2021 American Association for the Advancement of Science.

OPERANDO TECHNIQUES TO REVEAL CATALYST DYNAMICS

To date, no single *operando* technique can capture the complete picture of catalyst dynamics. By combining *operando* EM, X-ray spectroscopy, and vibrational spectroscopy, researchers can probe distinct aspects of catalyst behavior, from atomic-scale structure to electronic states and molecular interactions. This section outlines how each method offers complementary insights and how their integration deepens our understanding of dynamic catalytic processes.

***Operando* Electron Microscopy for Imaging Atomic and Morphological Transformations.** *Operando* electron microscopy (EM), primarily utilizing scanning and transmission electron microscopy (S/TEM), offers unparalleled spatial (~0.5 Å)[19] and temporal (~1 ms down to subps) resolution.[20,21] This technique enables near-real-time, nanoscale visualization of catalytic processes under working conditions. One of the key strengths of *operando* EM lies in its multimodal capabilities: it simultaneously acquires structural and chemical information through imaging, diffraction, and spectroscopy modes. By replicating realistic catalytic environments, including exposure to reactive gases or liquids, elevated temperatures, electrical bias, and even light stimuli, *operando* EM captures a wide range of dynamic phenomena such as morphology evolution, crystallographic transformations, atomic rearrangements, changes in size and shape distributions, and compositional shifts.[4,18,22−32] These diverse capabilities, coupled with high spatial and temporal resolution, make *operando* EM a uniquely comprehensive tool for studying catalyst dynamics at multiple scales and dimensions, enabling insights into mechanisms such as sintering, phase transitions, metal−support interactions, and degradation processes that are otherwise challenging to capture.

Operando EM has proven especially powerful for studying catalyst dynamics in gas-phase environments, where precise control over gas composition and temperature enables real-time observation of structural and compositional changes under reactive conditions.[23,26,33−41] Through this approach, *operando* EM has captured key gas-phase dynamics such as compositional evolution,[42] sintering via Ostwald ripening and coalescence,[43,44] and interaction between metal nanoparticles and the support.[45−49] More recently, Frey et al. used *operando* EM to investigate the dynamics of Pt nanoparticles on a TiO_2 support under H_2 and O_2 environments, capturing strong metal−support interaction (SMSI), a key phenomenon in catalyst dynamics. They showed that SMSI between Pt and TiO_2 is highly dynamic and reversible, depending on the redox conditions. Under mixed H_2/O_2 environments, redox-driven reconstructions of TiO_2 destabilize the interface and cause orientation-dependent particle migration, indicating that active sites can shift significantly during reaction[50] (Figure 2a). Researchers have also integrated conventional 2D STEM imaging with secondary electron-based 3D topological mapping to capture the spatial complexity of supported catalysts. For instance, Lee et al.[51] (Figure 2b) showed the sintering of Pt nanoparticles and localized degradation of the carbon support using the combined 2D and 3D images via high-angle annular dark-field STEM (HAADF-STEM) and secondary electron (SE) imaging equipped with differential pumping for gas flows and temperature control up to 700 °C. These advances highlight how *operando* EM in gas environ-

https://doi.org/10.1021/acsnano.5c10976
ACS Nano XXXX, XXX, XXX−XXX

ments provides a multidimensional view of catalyst evolution, essential for decoding deactivation mechanisms and designing stable, high-performance catalysts.

In parallel with advances in gas-phase *operando* EM, substantial progress has been made in extending *operando* EM capabilities to liquid-phase environments to study electrocatalyst dynamics under realistic electrochemical conditions.[52−58] By integrating liquid flow systems with electrochemical biasing, *operando* EM enables direct visualization of composition and phase evolution processes, which are the major contributors to the performance and degradation of electrocatalysts.[59−65] For example, a recent study by Kim et al. elucidated the degradation pathways of Pt on carbon electrocatalysts during accelerated stress test cycles for fuel cell applications, which are responsible for the oxygen reduction reaction (ORR). The authors periodically altered the liquid electrolyte thickness to obtain both a high-resolution image and signal from electrochemical biasing. From these results, they quantified the degradation process of the catalyst, revealing that smaller nanoparticles are more prone to migration and coalescence, giving insights into size-dependent durability (Figure 2c).[66] Moreover, diffraction such as 4D-STEM can be combined with imaging to elucidate the morphological evolution in complex catalytic structures.[67] For example, Yang et al. have shown the presence of metallic Cu grains for electrochemical CO_2 reduction reactions (CO2RR) using 4D-STEM images, showcasing the technique's ability to correlate phase transformation with electrocatalytic function (Figure 2d).[68] Ongoing developments are addressing critical challenges in *operando* liquid-phase EM to evaluate electrocatalyst dynamics correctly. For example, the electron beam effect on the solution chemistry of the liquid environment during *in situ* and *operando* environments is often considered challenging, but the pathways to overcome and exploit them were also reviewed in a recent review article by Fritsch et al.[69,70] Moreover, temperature control also functions as a critical parameter in electrocatalysis, and traditional efforts in implementing temperature control in liquid-phase TEM to analyze the kinetics of the reaction[71−76] were incorporated with electrochemical biasing to realize simultaneous temperature control and biasing.[62,77,78]

In addition to traditional external stimuli such as gas, liquid, temperature, and electrical biasing, light illumination has recently emerged as a powerful tool in *operando* EM for probing photocatalyst dynamics.[79] The integration of light into high-energy-resolution aberration-corrected STEM, enabled by innovations such as the cryo-cathodoluminescence holder developed by Vadai et al., allowed researchers to directly identify optically active catalytic sites by coupling optical excitation and collection with electron imaging.[80] This optically coupled setup, which uses dual optical fibers and parabolic mirrors surrounding the sample with a central aperture for the electron beam, revealed critical light-driven phenomena, such as the kinetics of Pd phase transformations during H_2 desorption/absorption[80] and plasmon-induced reaction localization at otherwise inactive sites (Figure 2e),[81] which demonstrates the unique capability of *operando* EM to uncover photocatalytic mechanisms that are inaccessible through conventional techniques.

Beyond imaging and diffraction, *operando* EM offers spectroscopic capabilities through techniques such as energy-dispersive X-ray spectroscopy (EDS) and electron energy loss spectroscopy (EELS), enabling comprehensive chemical analysis alongside structural observations.[82] These spectroscopies are critical for understanding catalyst dynamics, as catalysts often involve multicomponent systems with evolving elemental compositions and bonding states during reactions. EDS allows for spatially resolved elemental mapping, providing insight into compositional changes linked to catalytic activity.[36,42,83] EELS is suitable for revealing bonding types and vibrational modes, and it has been found particularly useful for catalyst reaction study as it can effectively quantify the gas product compositions for *operando* TEM study of the catalyst, which was demonstrated by Crozier et al.[84] High-resolution EELS can also extract the response from adsorbates on the catalyst surfaces. This is particularly important as the information on the bonding of the adsorbate−surface interface is the core of the catalyst activity.

Despite its powerful capabilities, *operando* EM has inherent limitations that can be complemented by other techniques. First, the intrinsic requirement for electron transparency constrains sample geometry, while electron beam-induced effects such as radiolysis remain a persistent concern in sensitive materials or liquid environments. Moreover, achieving atomic resolution under realistic operating conditions, such as high-pressure or high-temperature gas environments or in thick liquid layers for electrochemical studies, can be technically demanding; often, these reactive environments compromise the image quality. Furthermore, the simultaneous application of multiple external stimuli including gas, liquid, heating, electrical bias, and light illumination, still poses challenges for implementation. Lastly, although *operando* EM excels at visualizing structural and morphological changes, it needs to be improved in capabilities for identifying reaction products or probing vibrational signatures, requiring integration with complementary tools such as mass spectrometry or vibrational spectroscopy. These challenges highlight the importance of a multimodal approach to fully understand complex catalytic systems under *operando* conditions.

***Operando* X-ray Spectroscopy for Characterizing the Local Environment and Electronic Structure.** Among X-ray spectroscopy techniques, X-ray absorption spectroscopy (XAS) serves as a powerful complement to electron microscopy. The technique offers quantitative insights into the local chemical environment, with fewer constraints on sample geometry, such as thickness, making it particularly suitable for bulk-scale analysis.[16,17,61,85−87] Widely adopted in catalysis research, XAS encompasses two main techniques: X-ray absorption near-edge structure (XANES), which probes electronic structure and oxidation states, and extended X-ray absorption fine structure (EXAFS), which reveals coordination numbers and bond distances.[85] With advances in *operando* reactor cell designs, *operando* XAS can now be conducted under realistic catalytic conditions.[17,86] *Operando* XAS has contributed significantly to our understanding of gas-phase catalytic systems such as CO_2 hydrogenation,[88] as well as in electrocatalysis, where complex, multistep charge transfer mechanisms and dynamic redox behavior present unique challenges.[85,86,89,90] In particular, *operando* XAS has elucidated the mechanisms of key electrochemical processes such as water splitting involving oxygen evolution reaction (OER) and hydrogen evolution reaction (HER)[91−93] and CO_2 reduction reactions (CO_2RR).[94−98]

It is important to note that *operando* XAS provides ensemble-averaged spectroscopic information, which limits its ability to directly correlate with catalyst dynamics in terms of

https://doi.org/10.1021/acsnano.5c10976
ACS Nano XXXX, XXX, XXX−XXX

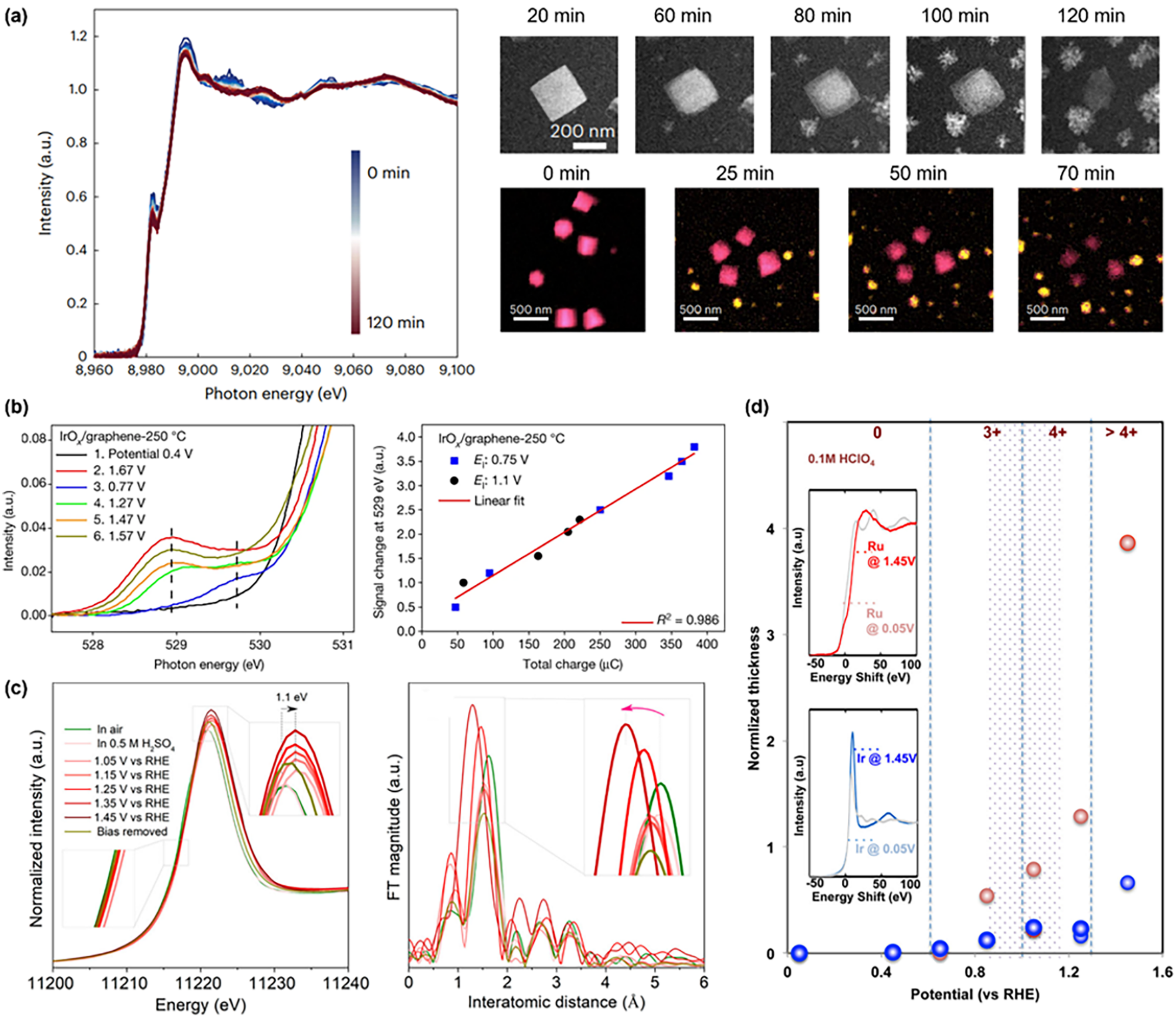

Figure 3. Probing the dynamic reaction mechanisms on the electrocatalytic interface using *operando* XAS. (a) *Operando* XANES measurement (left) paired with *operando* EM (top right) and XM (bottom right) on the Cu_2O catalyst under operating conditions of NO_3RR. (b) Steady-state *operando* XAS measurements on IrO_x/graphene OER catalysts with different applied voltages (left), showing the correlation of the charge accumulation to the electrochemical current (right). (c) *Operando* XANES (left) and EXAFS (right) spectra during OER using the Li-IrO_x catalyst showing the key role of the [IrO_6] hydrophilic center in promoting the reaction. (d) *Operando* XANES revealing the role of Ru and Ir in balancing reactivity and stability for OER. Adapted with permission from ref 107. Copyright 2020 Springer Nature.

structure and morphology. However, this limitation can be effectively complemented by *operando* EM, which offers atomic-to-nanoscale spatial resolution.[99,100] For example, recent work by Yoon et al.[61] demonstrated the synergistic effect of combining *operando* XAS, EM, and X-ray microscopy (XM) in revealing the evolution of Cu_2O structure and morphology, as well as its role in electrocatalytic performance for the nitrate reduction reaction (NO_3RR) (Figure 3a).

Operando XAS has been extensively applied to investigate the dynamics of OER, particularly in the context of water splitting using the acidic polymer electrolyte membrane, where OER presents a unique bottleneck due to its sluggish kinetics, high overpotentials, and harsh operating conditions.[101] These challenges have driven many research groups to utilize *operando* XAS to establish structure–activity relationships and identify stable, efficient catalysts under realistic operating conditions.[102−106] Jones' group demonstrated through combined pulse voltammetry and *operando* XAS that charge accumulation within iridium oxide catalysts, rather than direct bias effects on the reaction coordinate, controls the electrocatalytically generated current, revealing the major mechanism to tune the electrochemical reactivity (Figure 3b).[107] Findings from *operando* XAS, including XANES and EXAFS, have also revealed the dependence of performance on the catalytic structure, in particular the superior performance of amorphous materials compared to their crystalline counterparts. Gao et al. investigated amorphous Li-IrO_x electrodes in acidic media, revealing that these materials achieve superior OER activity due to their "flexible" disordered [IrO_6] octahedrons (Figure 3c).[108] Unlike the "rigid" periodically interconnected octahe-

https://doi.org/10.1021/acsnano.5c10976
ACS Nano XXXX, XXX, XXX−XXX

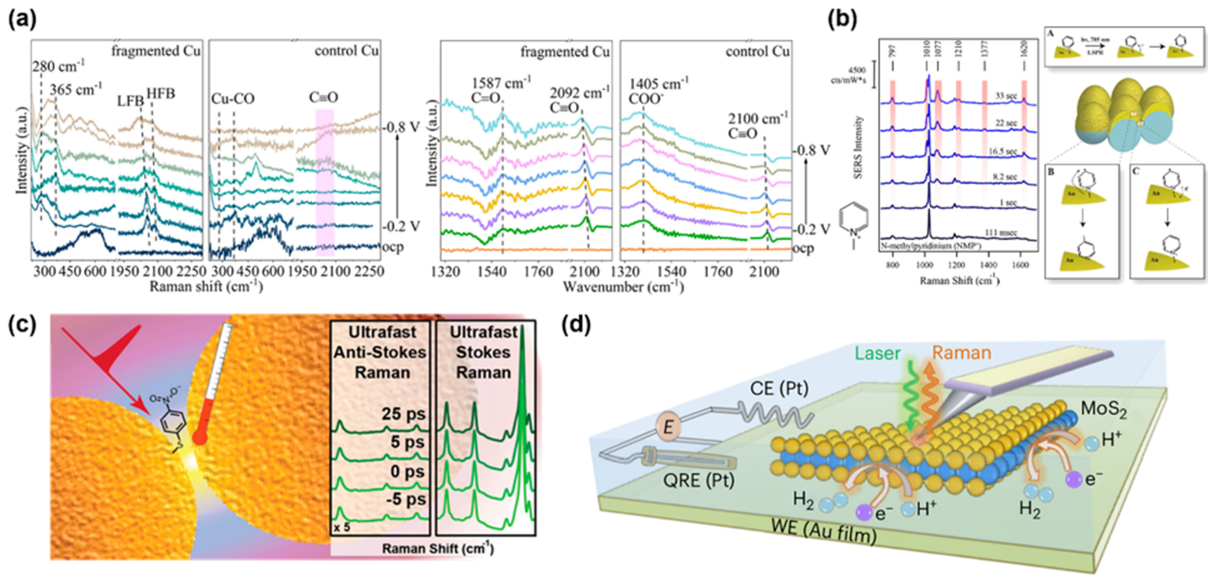

Figure 4. Molecule fingerprints, time-resolved dynamics, and nanoscale spatial resolution structural change enabled by *operando* vibrational spectroscopy. (a) *Operando* Raman spectroscopy (left) and FTIR (right) of fragmented Cu and control Cu catalysts at the various applied potential for the selective ethylene production from CO_2 reduction. (b) Time-resolved evolution of the plasmon-intermediate chemical conversion of *N*-methylpyridinium on an Au-film-on-nanosphere substrate. (c) Schematic illustrating picosecond-resolution Raman thermometry used to probe the local temperature of molecules at the gap of plasmonic gold (Au) structures. (d) Schematic of the experimental setup of EC-TERS, featuring the counter electrode (CE) and working electrode (WE). Adapted with permission from ref 119.

drons in crystalline IrO_2, these flexible structures undergo oxidation to higher Ir oxidation states and Ir−O bond contraction during OER conditions, creating more hydrophilic centers that facilitate water oxidation turnover.

Insights from *operando* XAS can also be applied to design new catalysts by learning which parameters tune the reactivity and stability of the catalysts. Danilovic et al. found that in acidic conditions, the valence is the key to the transition metal cations for electrochemical OER.[109] The high valence usually exhibits great reactivity but instability in OER, and vice versa. Through the interrogation of Ru and Ir catalysts, the intermediate oxide state of these metals improved the balance between the reactivity and stability (Figure 3d). Kim et al. enhanced OER performance by anchoring metallic Co nanoparticles onto yttrium ruthenate pyrochlore oxide.[110] Their *operando* XAS measurements identified that facile oxidation of Y and Ru cations under reaction conditions reduces the formation energy of critical [CoOOH] intermediates, thereby promoting catalytic activity. These studies collectively demonstrate how *operando* XAS reveals the dynamic nature of active sites, where local coordination environment changes and oxidation state transitions directly control catalytic reactivity.

***Operando* Vibrational Spectroscopy for Analyzing Chemical Bonds and Adsorbates.** While *operando* EM and XAS probe the structure and electronic configuration of the catalyst itself, vibrational spectroscopy excels in detecting the chemical identity and dynamics of molecular species interacting with catalyst surfaces. Infrared vibrational spectroscopy, such as Fourier-transform infrared spectroscopy (FTIR) and surface-enhanced Raman spectroscopy (SERS), probes the molecular structural information, i.e., fingerprints, from vibrational modes with frequencies typically at 4000−400 cm^{-1}. These techniques are complementary to XAS, enabling the detection of dynamic adsorbate evolution on the catalyst surface and at solid−liquid or solid−gas interfaces. Therefore, vibrational spectroscopy adds a molecular-scale dimension to *operando* studies, capturing dynamic interactions at the solid−liquid or solid−gas interface that directly govern catalytic performance. Similar to XAS, these methods have been instrumental in real-time tracking of catalytic pathways by identifying adsorbed intermediates in electrochemical processes, including water splitting[93,111,112] and CO_2RR.[95,97,111] For example, Yao et al.[113] designed a fragmented Cu catalyst with a low coordination number to enhance C−C coupling for CO_2 reduction. Using *operando* FTIR and SERS in a CO_2-saturated 0.1 M $KHCO_3$ solution, they investigated the regulation of Cu−CO accumulation under different potentials. Their analysis revealed the C=O stretching mode of *OCCOH intermediates, distinguishing the behavior of low-coordination Cu from conventional Cu catalysts (Figure 4a).

Beyond its specificity in identifying molecular fingerprints, SERS offers exceptionally high sensitivity, enabling detection down to the single-molecule level.[114] Brooks et al.[115] monitored the plasmon-driven intramolecular methyl migration of *N*-methylpyridinium (NMP) to 4-methylpyridine (Figure 4b). SERS was crucial for confirming the product's identity by comparing experimental spectra with theoretical studies and revealing the dependence of reaction yield on the laser focus position. The analysis highlighted how the distribution of enhanced electromagnetic fields on the plasmonic Au-film-overnanosphere substrate influenced reaction efficiency, with steric hindrance playing a crucial role at the laser focus. SERS can also be applied in the study of photocatalytic systems in nature, such as photosynthesis. For example, Wilson and Jain used SERS to find the intermediate states and the reaction cycle of the light-driven water splitting catalyzed by the oxygen-evolving complex, which emphasized the role of low-frequency SERS as a critical tool for elucidating the catalyst dynamics.[116]

https://doi.org/10.1021/acsnano.5c10976
ACS Nano XXXX, XXX, XXX−XXX

Vibrational spectroscopy also benefits from ultrafast temporal resolution, allowing for the study of reaction kinetics on the picosecond timescale and offering unique insight into energy dissipation mechanisms during photochemical reactions. Keller and Frontiera[117] first measured the effective temperature on the probe molecule at the Au dimer junction, which is an electromagnetic hotspot under light irradiation (Figure 4c). Through the measurements of the ultrafast Stokes and anti-Stokes thermometry with the illumination condition at peak flux values 10^8 times stronger than the focused sunlight, the effective photothermal heating is less than 100 K and dissipates within ∼5 ps. This experimental observation shows that photothermal heating is not a primary mechanism for plasmon-driven chemistry. Other infrared spectroscopies, such as infrared transient absorption spectroscopy, can also provide valuable insights into the dynamics of the light-driven reaction of photocatalysts. For example, Tagliabue et al. employed ultrafast infrared transient absorption spectroscopy to reveal the hot-carrier dynamics in metal−semiconductor heterostructures, which can serve as a foundation for designing photocatalysts on ultrafast timescales.[118]

Moreover, advanced forms of Raman spectroscopy, such as electrochemical tip-enhanced Raman spectroscopy (EC-TERS) equipped with a sharp metallic tip for nanoscale resolution, can provide enhanced surface-sensitive characterization of electrochemical processes and catalytic reactions. For example, Huang et al.[119] used EC-TERS with 7.3 nm spatial resolution to study the structural evolution of MoS_2 during the HER (Figure 4d). They revealed that lattice deformation and electron density variations extend from the edge into the basal plane, with performance enhancements attributed to irreversible reconstructions from sulfur atom loss, facilitating hydrogen adsorption and reducing activation energy. In summary, vibrational spectroscopy with its high sensitivity, molecular specificity, and high temporal and spatial resolution has become a powerful tool for investigating molecular structures, dynamic processes, and interactions.

Together, these *operando* techniques form a complementary suite that links structure, electronic state, and interfacial chemistry across spatial and temporal scales. Their integration enables a comprehensive view of catalyst dynamics that no single technique can provide alone, setting the stage for theory-guided interpretation and data-driven discovery described in the following sections.

Theoretical Approaches to Link *Operando* Analysis and Computational Modeling. Ab initio calculations have become a cornerstone of catalysis research, as these calculations offer insights into surface chemistry and reaction mechanisms. Since the foundational work by Nørskov and coworkers in the early 2000s, DFT has enabled qualitative insights across a wide range of materials, from symmetric, single-element metals to complex multielement systems, such as oxides, perovskites, and transition metal dichalcogenides.[120−123] However, its predictive accuracy remains limited by the difficulty of capturing realistic operating conditions. It is often challenging to incorporate key factors affecting the reactant binding energies, such as surface reconstruction, solvation, and local electric fields, into the standard DFT frameworks. Most simulations still rely on idealized, energetically stable surface models that differ significantly from the dynamic, heterogeneous surfaces under *operando* conditions. Even noble metals, which are often regarded as chemically stable, undergo substantial restructuring under reaction environments. Migration, dissolution, and oxidation processes are frequently observed during operation, and these transformations diverge considerably from idealized surfaces, thereby complicating predictive modeling. Furthermore, recent theoretical studies have revealed that catalytic activities are often dominated not by these majority stable sites but by minority or transient active sites, which emerge dynamically and transiently under reaction conditions.[124−127] These sites, though challenging to directly observe using conventional experimental techniques, which primarily capture only abundant majority sites, play a critical role in driving catalytic performance. Pioneering researchers have extensively combined advanced computational modeling with *operando* experimental techniques to unearth these elusive active sites and demonstrate their significant impact. This growing body of work highlights the inherent limitations of static models and underscores the need for integrated theoretical−experimental frameworks that can accurately capture the evolving microenvironment and transient phenomena at the local catalyst surface.

In this context, the *operando* techniques described above are powerful tools for directly probing active sites, reaction intermediates, and the evolving catalyst surface microenvironment under realistic operating conditions. These experimental insights serve not only as validation points but also as essential baselines for refining ab initio calculations. Complementarily, theoretical modeling continues to provide critical information that remains experimentally elusive, such as reaction energy landscapes,[128] hybrid molecular-catalyst orbitals,[129,130] and catalyst−substrate interactions.[131,132] Recent efforts have increasingly focused on closing the gap between simulations based on ideal static models and dynamic systems under realistic operating environments by integrating observations from *operando* studies and computational modeling. The focus of computational−experimental integration is defined in stages of (1) precise prediction of the catalyst surface structure, (2) identification and theoretical validation of reaction intermediates, and (3) investigation of the influence of the microenvironment on catalyst behavior.

Understanding the precise atomic structure and activity of catalytic sites is foundational for unraveling reaction mechanisms and guiding catalyst design.[127] In this context, surface-sensitive techniques such as scanning tunneling microscopy (STM), combined with computational modeling, have been instrumental in providing atomic-level insights under well-controlled conditions. The works led by Hammer and coworkers highlight the importance of accurately identifying active edge sites and elucidating diffusion and adsorption behaviors on model catalysts, such as single-layer MoS_2 and anatase TiO_2 surfaces.[133−135] These studies underscore how detailed surface site characterization, including adsorbate interactions and dynamic surface rearrangements, is critical for constructing reliable reaction site models that inform both experimental interpretation and theoretical predictions. Advanced imaging techniques, particularly *operando* EM, enable real-time visualization of surface atom arrangements and dynamic reconstructions that are otherwise inaccessible. These observations provide definitive structural evidence that bridges theoretical predictions with experimental reality. Avanesian et al. presented the surface reconstruction mechanism of Pt nanoparticles under elevated temperature with CO gas.[39] High-resolution STEM (HRSTEM) images revealed Pt migration upon CO exposure, resulting in the

https://doi.org/10.1021/acsnano.5c10976
ACS Nano XXXX, XXX, XXX−XXX

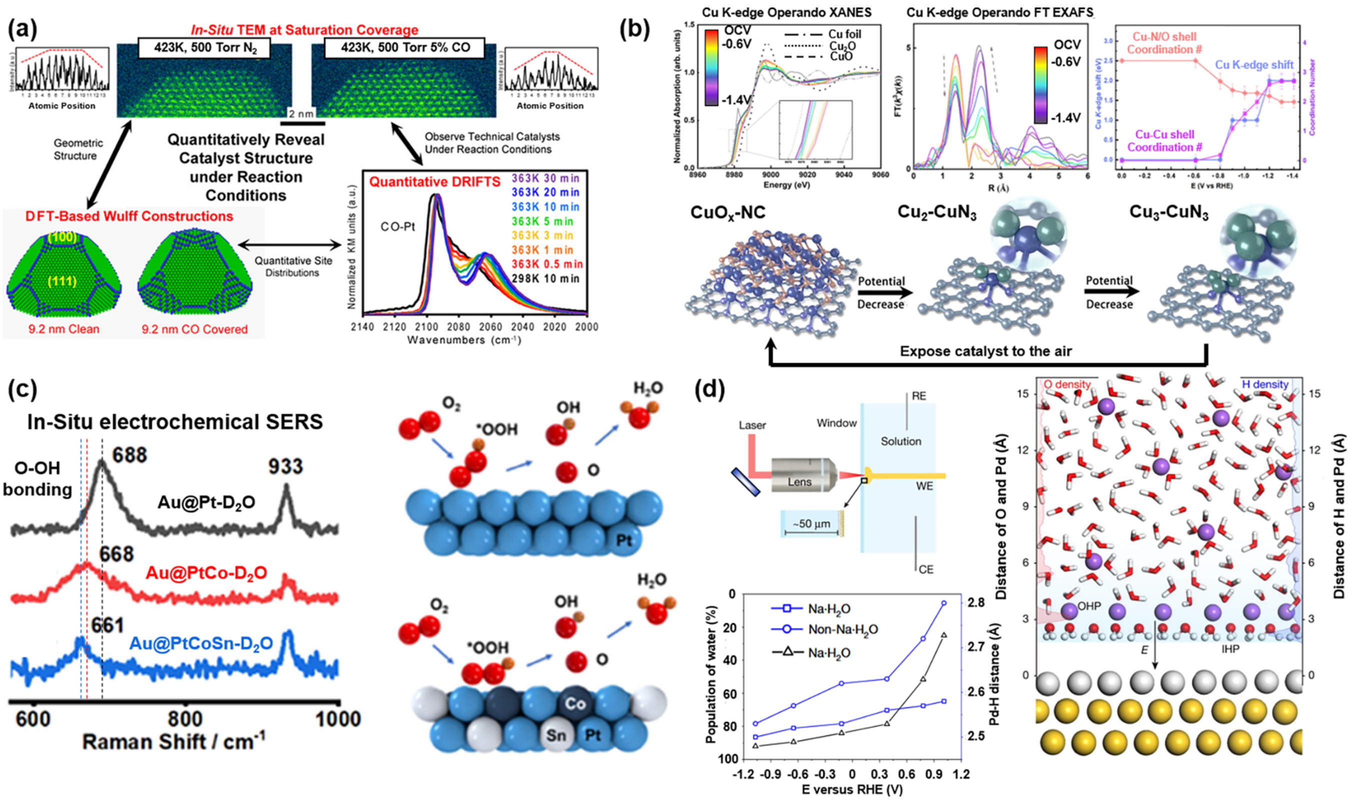

Figure 5. Synergetic collaboration of *operando* analysis and computational materials science. (a) Scheme of the observation of Pt nanoparticles under CO condition through *operando* TEM, DRIFTS, and DFT simulation-based Wulff constructions. (b) Cu K-edge *operando* XANES and FT-EXAFS of Cu/$N_{0.14}$C and proposed scheme for reversible formation of CuN-CuN_3 clusters. (c) *Operando* electrochemical Raman spectra of Au@Pt, Au@PtCo, and Au@PtCoSn with the scheme of ORR steps on Pt and the PtCoSn alloy. (d) Schematic of the Raman setup and the interfacial model of the Pd/Au surface with the calculated Pd−H distance and Na·H_2O population. Adapted with permission from ref 153. Copyright 2021 Springer Nature.

transformation of the (100) surface into high-index facets (Figure 5a). This structural evolution was supported by DFT simulations, which showed that CO adsorption more significantly stabilizes the surface energy of high-index facets compared to the (100) surface. The stabilization of the structure through Pt migration was further corroborated by diffuse reflectance infrared Fourier-transform spectroscopy (DRIFTS), which revealed a time-dependent increase in the vibrational signal of CO on undercoordinated Pt (~2060 cm^{-1}), typically found on high-index surfaces. Similarly, Vara et al. investigated the deformation of Pd−Pt core−shell nanoparticles under high temperatures. *Operando* STEM analysis showed that cubic nanoparticles maintained their core−shell structure even at high temperatures of 900 °C, whereas octahedral particles lost their core−shell architecture due to Pt diffusion at 600 °C. Based on these observations, the mechanism of core−shell structure reconstruction was investigated, revealing that the activation barrier for subsurface vacancy-mediated inward diffusion of surface Pt atoms is higher in cubic nanoparticles compared to octahedral ones.[136]

The surface electronic structure plays a central role in governing the adsorption behavior and reaction pathways. Subtle changes in the electronic configuration, such as d-band center shifts, charge redistribution, and local work function variations, can significantly alter reaction energetics. These changes directly impact the accuracy of computational models, as electronic structure descriptors are often used to parametrize adsorption energies and activation barriers in DFT simulations.[137] For example, variations in surface coordination or local charge redistribution can shift adsorption energies by several electron volts, directly influencing predicted reaction mechanisms and rate-determining steps. Therefore, incorporating experimentally derived electronic structure data into simulation workflows is essential for improving the computational models to reflect the real catalytic environments. One key aspect of reaction environment-dependent electronic structure is the dynamic interaction between the catalyst and substrate. Recent studies using *operando* spectroscopy have captured such substrate-induced electronic modulations, providing essential descriptors for mechanistic simulations. Rousseau's group revealed that substrate−catalyst interactions fundamentally modulate the electronic structure of single-atom active sites, stabilizing them through charge transfer mechanisms that enhance catalytic activity.[131,132] Their findings showed that increasing the density of active sites can lead to cumulative electronic effects, causing overactivation and the depletion of reactive species, which ultimately diminishes catalyst performance. Complementing this, studies on catalyst systems supported on another substrate demonstrated that dynamic restructuring of the active metal atoms, driven by interactions with the support under reaction conditions, shifts electronic states and adsorption properties, thereby tuning reaction energetics and improving activity. *Operando* spectroscopic techniques provided direct observation of real-time changes in atomic coordination and oxidation states under working conditions, while complementary DFT calculations quantitatively linked these changes to adsorption energies and reaction barriers, verifying their direct impact on catalytic

https://doi.org/10.1021/acsnano.5c10976
ACS Nano XXXX, XXX, XXX−XXX

performance. Friebel et al. also combined observations from *operando* XAS and DFT to investigate a Pt monolayer supported on a Rh(111) substrate. Their results showed that compressive strain and ligand effects from the Rh underlayer lead to a downshift in the Pt d-band center, which suppresses the Pt oxidation.[138] A similar modulation of the surface electronic structure by the underlying substrate has also been reported in CO_2RR systems. A representative example is the formation of $Cu^0Cu^{\delta+}$ pair sites during electrochemical CO_2RR, as reported in a recent study by Zhang et al. on exsolved Cu nanoclusters supported on $CaCO_3$. Using *operando* XAS, they revealed the coexistence of metallic Cu and partially oxidized $Cu^{\delta+}$ species under reaction conditions. DFT calculations showed that strong interactions between Cu and the carbonate support stabilize this mixed-valence state by suppressing complete reduction, thereby enhancing C−C coupling activity.[139] Similarly, Su et al. investigated the structural evolution of Cu-based catalysts during CO_2RR, focusing on the coordination environment of Cu under varying potentials.[140] *Operando* XAS showed that a negative bias induces a transition from Cu−N coordination to the formation of Cu−Cu bonds, leading to the generation of Cu_x-CuN_3 (x = 1−3) active sites (Figure 5b). These structural changes were inferred from *operando* electronic structure signatures from XAS and served as the basis for subsequent DFT simulations. Theoretical analysis showed that the Cu_2−CuN_3 site exhibits the optimal balance between adsorption strength and intermediate stabilization for C−C coupling, consistent with the experimentally observed maximum ethanol Faradaic efficiency at −1.1 V, where the coordination structure of the Cu_2−CuN_3 motif dominates.

Beyond identifying the catalyst surface structure, investigating the actual reaction pathway remains one of the most challenging and time-consuming tasks in theoretical catalyst evaluation. For simple reactions such as HER, the mechanism can be categorized into well-established two-step pathways, like the Volmer−Heyrovsky or Volmer−Tafel pathways, making simulations relatively straightforward. However, for more complex reactions such as CO_2RR, the diversity of possible products leads to multiple competing pathways, each with different intermediates and binding configurations. Even for a single product, there often exist controversies regarding the nature of key intermediates and their adsorption geometries.[141] To address this uncertainty, integration with *operando* vibrational spectroscopy techniques, such as FTIR and Raman spectroscopy, has proven invaluable.[142] These methods can directly capture the vibrational signatures of adsorbed reaction intermediates, especially those involved in the rate-determining step. By experimentally identifying these key species, the scope of DFT simulations can be significantly narrowed, focusing on the energetics of the most relevant steps. For instance, Zhong et al. reported a collaborative study on improving ORR activity by alloying Sn and Ag into a Pt-based catalyst.[143] *Operando* SERS revealed a peak shift associated with weakened O−OH bonding in the *OOH intermediate (Figure 5c). Based on this observation, DFT simulations showed that the introduction of Co further promotes *OOH destabilization, facilitating O−O bond formation and accelerating the subsequent steps of ORR.

Understanding catalytic performance requires consideration of reaction microenvironments, such as the interfacial solvent structure,[144,145] local ion effects,[146] and electrolyte dynamics.[147,148] These microenvironments profoundly influence catalytic performance by modulating key interfacial processes. The arrangement and orientation of solvent molecules at the catalyst interface can affect reactant adsorption, intermediate stabilization, and charge transfer pathways, thereby altering catalytic activity and selectivity. Local ion concentrations and distributions create specific electrostatic environments that can promote or hinder reaction steps, impact proton-coupled electron transfer, and influence the formation of reaction intermediates.[149,150] Additionally, electrolyte dynamics govern mass transport and the distribution of reactive species near the catalyst surface, affecting reaction kinetics and stability under operating conditions.[151] Despite its importance, integration of experimental *operando* studies and theory at the microenvironment level remains relatively underexplored, and the corresponding analytical techniques are less standardized compared to surface-level studies. Simulation approaches at this scale often move beyond DFT, utilizing MD, COMSOL, or finite-difference time-domain (FDTD) methods to capture mesoscale behaviors. A representative example is the recent work by Candeago et al. combining *in situ* neutron reflectometry with ab initio MD, which revealed how solvation structures and ion valency dictate redox-mediated electrosorption phenomena at electrified interfaces.[152] This study exemplifies how theory and *operando* experiments together can resolve solvent−ion interactions inaccessible to static DFT models. In particular, the neutron reflectometry measurements provided interfacial solvent layering and ion distribution profiles, which were subsequently incorporated into the AIMD simulations to reproduce redox-mediated electrosorption events under realistic conditions. In a related direction, Wang et al. investigated the structure and dynamic evolution of interfacial water on Pd single-crystal surfaces using *operando* Raman spectroscopy and MD simulations (Figure 5d).[153] They demonstrated how applied bias and Na^+ ion interactions induce an ordering transition in interfacial water, enhancing hydrogen bonding and orienting water dipoles toward the Pd surface. This restructuring, supported by MD results, promotes more efficient charge transfer in HER by reducing the Pd−H distance. In follow-up work, Wang et al. proposed a systematic protocol integrating *operando* electrochemical Raman spectroscopy and ab initio MD for studying interfacial water structures.[154] *Operando* EM can also be used to explore interfacial structures, as demonstrated by the work of Peng et al., which investigated the quasi-liquid-phase behavior at the solid−liquid interface of In nanoparticles, drawing insights from liquid-phase TEM.[155] Through MD simulations, they found that only positively charged In ions, not neutral In atoms, can sustain a stable quasi-liquid state, highlighting the critical role of charge in interfacial phase stability. Yang et al. employed *operando* confocal microscopy to investigate catalyst flooding behavior in fuel cells.[156] They observed that droplets formed only on the ion-generating side, such as during alkaline ORR or acidic hydrogen oxidation reaction (HOR). MD simulations confirmed this mechanism by showing that ion-rich interfaces facilitate water agglomeration, with alkaline conditions producing larger droplets than acidic ones. Extending beyond the catalyst surface itself, the concept of microenvironment engineering has expanded to include the design of membranes and solvent interfaces that control mass transport and reactant flux on larger spatial scales. With the widespread adoption of membrane electrode assembly (MEA) cell structures, the microenvironment within the membrane region has emerged as a critical factor

https://doi.org/10.1021/acsnano.5c10976
ACS Nano XXXX, XXX, XXX−XXX

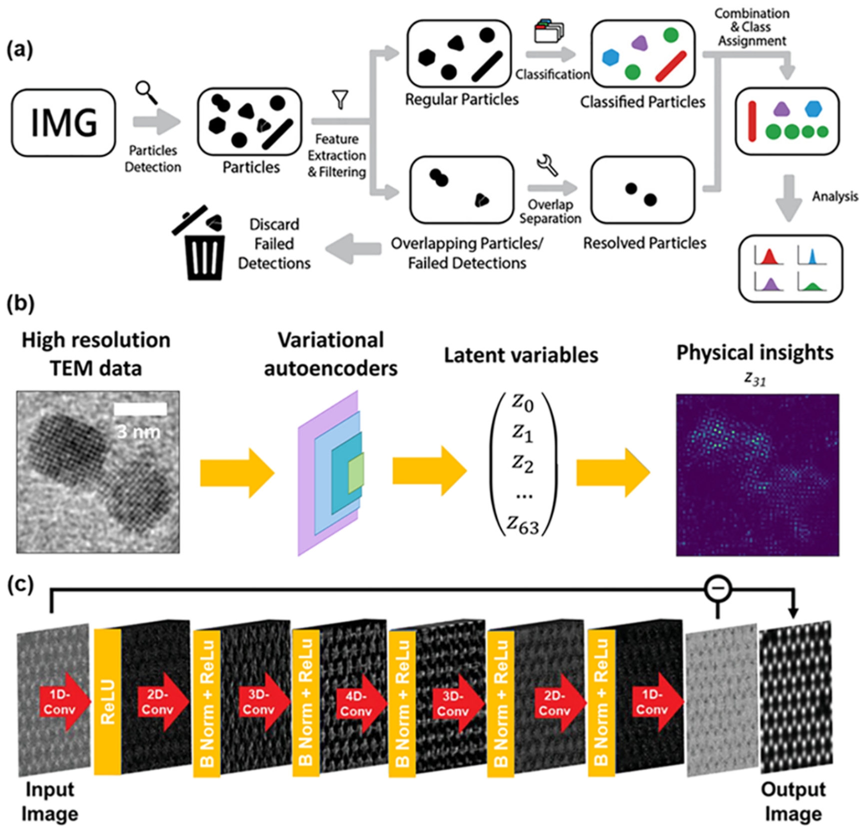

Figure 6. Contribution of ML-based data analysis to *in situ* and *operando* techniques. (a) Schematic of the AutoDetect-mNP algorithm. (b) Scheme of deconvoluting physically meaningful information from electron microscopy data. (c) Deep neural network model constructed for the denoising process for the ADF STEM image of WSe_2. Adapted with permission from ref 182. Copyright 2021 Wiley.

influencing overall catalytic efficiency. Walter et al. revealed molecular-level interactions and dynamic rearrangements occurring at the membrane-solvent-CO_2 surface with NMR spectroscopy and MD simulations.[157] Their findings demonstrate that CO_2 induces molecular reorganization at this boundary, creating transient pathways that significantly enhance CO_2 diffusion across the solvent interface. Additionally, carbamic acid species formed during CO_2 capture disrupt ionic cross-linking within the membrane, further facilitating CO_2 transport.

Machine Learning Integration in *Operando* Analysis Workflows. Prior to its integration with *operando* studies, ML had already become a valuable tool in catalysis research more broadly. Applications span from global atomic structure optimization, where ML accelerates the exploration of complex potential energy surfaces and the identification of stable or metastable configurations, to the prediction and exploration of catalytic reaction networks, the discovery of chemically meaningful descriptors, and the reduction of complexity in modeling heterogeneous catalytic systems.[158−160] While these studies highlight how ML has traditionally been used to accelerate modeling and mechanistic understanding, in the following, we focus on a different but increasingly important direction: the application of ML to the analysis of complex *operando* data sets. The increasing complexity and volume of the data generated by *operando* techniques have outpaced the capacity of manual quantification and interpretation, prompting a shift toward computational approaches. In this context, ML methods have emerged as a powerful solution for automating the analysis of data from *operando* experiments. ML offers several distinct advantages over conventional manual methods. It enables high-throughput processing, allowing rapid analysis of large data sets that would otherwise demand extensive time and labor. Moreover, ML minimizes human-induced variability by applying consistent algorithmic criteria, thereby enhancing the standardization and reproducibility of data analysis. Multimodal data interpreted by ML can also lead to automated experimentation, where real-time analysis of outputs can dynamically inform and optimize subsequent experimental parameters, significantly expediting experiment optimization, such as by designing data-driven EM architecture.[161]

Building on these advantages, ML methodologies have been applied across a wide range of *operando* data types to enable efficient, large-scale quantification. In spectroscopic investigations, ML algorithms have been used to identify and quantitatively track temporal variations in Raman spectroscopy peak intensities associated with specific reaction intermediates or products.[162,163] Within the domain of imaging, particularly *operando* TEM, ML facilitates extensive quantification tasks, including automated detection, classification, and morphological analysis of catalyst nanoparticles.[164] Notably, Wang et al. developed the AutoDetect-mNP algorithm, an unsupervised machine learning approach that classifies Au nanoparticles based on multiple shape descriptors such as area, eccentricity, aspect ratio, and circularity from bright-field TEM images (Figure 6a).[165] Beyond morphological quantification, ML methods have been employed in high-resolution electron microscopy to extract crystallographic details and identify atomic-scale structural transformations, extending analysis down to crystal phases and defect states.[166,167] In addition to these static measurements, time-resolved EM studies have leveraged ML to analyze image sequences in real time, enabling the automated tracking of catalyst dynamics and interactions during reactions.[168−170] As these applications advance toward increasingly fine spatial resolution and dynamic temporal analysis, a persistent challenge emerges: the scarcity of well-annotated training data sets needed to develop reliable segmentation models. To address this, Vuijk et al. have introduced a physics-based synthetic data generation framework that produces realistic electron microscopy images for training, thereby enhancing the accuracy and robustness of automated segmentation in catalysis microscopy.[171]

Beyond data quantification, machine learning also plays a pivotal role in the interpretation of *operando* data sets, extracting a mechanistic understanding of dynamic catalytic reactions. In *operando* XAS, where signal variations are often subtle due to low catalyst loading and environmental interference, ML provides a systematic approach to decode complex spectral features. While most ML applications have focused on XANES, efforts to apply these methods to EXAFS are emerging.[172] A common strategy involves combining ML, either supervised or unsupervised, with ab initio simulations to match theoretical and experimental spectra.[173,174] This enables the identification of key structural parameters such as the oxidation state and coordination number under realistic reaction conditions. Some studies further leverage ML to uncover structure−activity relationships, identifying descriptors that govern catalytic performance.[175] In imaging studies, ML has also been applied to interpret real-time high-resolution TEM data. Wang et al. employed variational autoencoders (VAEs), an unsupervised machine learning model, to analyze in *operando* HRTEM image sequences of nanocrystals. The model extracted latent variables that correspond to physically meaningful nanoscale phenomena such as lattice rotations and particle ripening, enabling automated and unbiased mechanistic interpretation without human supervision (Figure 6b).[176]

Such ML-driven insights into reaction mechanisms and active site dynamics can further serve as a foundation for *de novo* catalyst design. Here, *de novo* refers to designing entirely new catalysts from first-principles rather than modifying existing ones. By integrating structural and electronic descriptors derived from *operando* data interpretation, generative models, including VAEs and diffusion-based architectures, can propose novel catalyst structures tailored to exhibit desired reactivity or selectivity. This approach parallels recent advances in protein design, where a mechanistic understanding informs the generation of functional biomolecules.[177−179] In catalysis, this strategy holds promise to rationally explore vast chemical spaces beyond conventional intuition-based design.[180]

In addition to data interpretation, ML also contributes to improving the quality of *operando* analyses. One of the major challenges in *operando* imaging lies in balancing realistic operating conditions with maintaining high spatial and temporal resolution. Increasing temporal resolution often requires sacrificing signal intensity, and the reactive environment may require low-dose imaging to minimize beam-induced radiolysis, which leads to noisy and blurred images.[181] To overcome these limitations, ML-based denoising techniques have been developed to enhance image quality, enabling the extraction of important structural information such as crystallinity, morphology, and atomic structure from raw data. Yang et al. proposed a convolutional neural network (CNN) denoiser for 2D transition metal dichalcogenide images, which isolates and subtracts statistical noise from annular dark-field images to restore true atomic contrast.[182] Through supervised training, this method successfully produced sharper, higher-quality images (Figure 6c). Efforts to advance such denoising algorithms continue actively, encompassing both supervised[183,184] and unsupervised[185,186] training.

CONCLUSIONS AND OUTLOOK

The advancement of *operando* techniques has fundamentally reshaped our understanding of catalyst dynamics by enabling real-time observation of structural, chemical, and physical transformations under realistic operating conditions. These approaches reveal that catalysts are not static entities but inherently dynamic systems that continuously respond to changes in potential, temperature, reactants, and local environments. This challenges conventional, static models of catalysis and emphasizes the need for frameworks capable of spatiotemporal complexity. Moreover, when combined with computational modeling, *operando* studies provide a powerful feedback loop, where experimental data inform and validate theoretical models, while simulations offer mechanistic insights that guide interpretation and further experimentation. Similarly, the integration of ML into *operando* workflows enables analysis of complex data sets, which facilitates the automated experiment design and discovery through data-driven feedback.

A compelling example of this integrative approach is the recent study on Cu nanocube catalysts under CO_2 reduction reaction (CO_2RR) conditions, which combined *operando* electrochemical liquid-cell STEM, synchrotron X-ray spectroscopy, ML-enhanced 4D-STEM, *in situ* Raman spectroscopy, and DFT calculations.[187] This multimodal framework revealed a complete structural transformation of (100)-faceted Cu@Cu_2O nanocubes into polycrystalline metallic Cu nanograins, with the extent and nature of reconstruction strongly dependent on particle size and applied potential. Importantly, ML-assisted 4D-STEM enabled nanoscale classification of crystalline vs amorphous grain formation, which gives insights not accessible via imaging or spectroscopy alone. At the same time, Raman and DFT uncovered CO-driven Cu atom ejection and migration pathways. This example mainly showcases how integrating multiple *operando* methods with theory and data can unravel complex catalytic dynamics inaccessible to any single technique.

Despite these advances, *operando* studies remain hindered by a lack of standardization. The diversity of experimental setups and data acquisition often leads to issues with reproducibility and compatibility across studies. In contrast to *ex situ* techniques, where analytical protocols are well-established and cross-validation is routine, *operando* studies still rely heavily on customized configurations, limiting their generalizability.[2] Establishing standardized protocols for measurement, data processing, and interpretation is therefore essential to ensure the reliability and interoperability of *operando* results. Equally important is the development of robust strategies for cross-validation across different *operando* techniques.

In addition to standardization, *operando* studies face several experimental and computational limitations that must be addressed to broaden their applicability and reliability. For example, electron beam-induced effects in *operando* EM, such

https://doi.org/10.1021/acsnano.5c10976
ACS Nano XXXX, XXX, XXX−XXX

as radiolysis and knock-on damage, can alter the intrinsic behavior of sensitive catalysts, especially in liquid or gas environments. Careful control of beam dose and understanding of the beam effect on the physical and chemical environment inside EM would be one avenue to mitigate this issue, along with other complementary measurements on different length-time scales for cross-validation. Variability in sample geometry and reaction conditions across *operando* platforms also complicates reproducibility, emphasizing the need for standardized protocols and cross-validation using complementary techniques. On the computational front, while machine learning has emerged as a powerful tool for high-throughput data analysis, model interpretability and generalizability remain open challenges. Transparent benchmarking, physically informed model constraints, and integration with theoretical frameworks like DFT can enhance robustness. Overall, addressing these limitations requires a combination of technical innovation, data standardization, and interdisciplinary collaboration.

Looking ahead, the integration of standardized protocols with automation and data-driven methods can open up a pathway to make *operando* studies on catalysis more reproducible, scalable, and impactful. High-throughput experimental *operando* platforms, coupled with ML-based data analysis and interoperable databases, will not only accelerate academic discovery but also contribute to the transition from isolated and fragmented case studies to systematic, generalizable insights. These developments will form the foundation for next-generation catalyst design, founded by reproducible science and powered by real-time, automated analysis pipelines.

AUTHOR INFORMATION

Corresponding Authors

Jennifer A. Dionne − *Department of Materials Science and Engineering, Stanford University, Stanford, California 94305, United States;* orcid.org/0000-0001-5287-4357; Email: jdionne@stanford.edu

Jungwon Park − *School of Chemical and Biological Engineering, Institute of Chemical Processes, Center for Nanocrystal Research, Institute for Basic Science (IBS), Institute of Engineering Research, College of Engineering, Advanced Institute of Convergence Technology, and Hyundai Motor Group-Seoul National University (HMG-SNU) Joint Battery Research Center (JBRC), Seoul National University, Seoul 08826, Republic of Korea;* orcid.org/0000-0003-2927-4331; Email: jungwonpark@snu.ac.kr

Authors

Tae Hyung Lee − *School of Chemical and Biological Engineering, Institute of Chemical Processes, Seoul National University, Seoul 08826, Republic of Korea*

Serin Lee − *Department of Materials Science and Engineering, Stanford University, Stanford, California 94305, United States;* orcid.org/0000-0002-3672-5076

Lin Yuan − *Department of Materials Science and Engineering, Stanford University, Stanford, California 94305, United States;* orcid.org/0000-0002-6426-0296

Complete contact information is available at: https://pubs.acs.org/10.1021/acsnano.5c10976

Author Contributions

[†]T.H.L. and S.L. contributed equally.

Notes

The authors declare no competing financial interest.

ACKNOWLEDGMENTS

J.P. and J.A.D. acknowledge financial support from the National Research Foundation of Korea (NRF) grant funded by the Korean Government (Ministry of Science and ICT) (No. RS-2024-00421181). Additionally, J.P. also acknowledges financial support from the Nano & Material Technology Development Program through the National Research Foundation of Korea (NRF) funded by Ministry of Science and ICT (RS-2024-00449629). J.A.D. and S.L. acknowledge the financial support from the U.S. Department of Energy Office of Science National Quantum Information Science Research Centers as part of the Q-NEXT center. J.A.D. and L.Y. acknowledge the financial support from the Basic Energy Sciences program by the U.S. Department of Energy (DE-SC0021984).

REFERENCES

(1) Shukla, P. R.; Skea, J.; Slade, R.; Al Khourdajie, A.; van Diemen, R.; McCollum, D.; Pathak, M.; Some, S.; Vyas, P.; Fradera, R.; Belkacemi, M. *Climate Change 2022: Mitigation of Climate Change. Working Group III Contribution to theSixth Assessment Report of theIntergovernmental Panel on Climate Change*; Cambridge University Press: **2022**, *10*, 9781009157926.

(2) Chavez, S.; Werghi, B.; Sanroman Gutierrez, K. M.; Chen, R.; Lall, S.; Cargnello, M. Studying, Promoting, Exploiting, and Predicting Catalyst Dynamics: The Next Frontier in Heterogeneous Catalysis. *J. Phys. Chem. C Nanomater. Interfaces* **2023**, *127*, 2127−2146.

(3) Ertl, G. Reactions at Surfaces: From Atoms to Complexity (Nobel Lecture). *Angew. Chem., Int. Ed. Engl.* **2008**, *47*, 3524−3535.

(4) Lundgren, E.; Zhang, C.; Merte, L. R.; Shipilin, M.; Blomberg, S.; Hejral, U.; Zhou, J.; Zetterberg, J.; Gustafson, J. Novel in Situ Techniques for Studies of Model Catalysts. *Acc. Chem. Res.* **2017**, *50*, 2326−2333.

(5) Weckhuysen, B. M. Determining the Active Site in a Catalytic Process: Operando Spectroscopy Is More than a Buzzword. *Phys. Chem. Chem. Phys.* **2003**, *5*, 4351−4360.

(6) Yang, Y.; Feijóo, J.; Briega-Martos, V.; Li, Q.; Krumov, M.; Merkens, S.; De Salvo, G.; Chuvilin, A.; Jin, J.; Huang, H.; Pollock, C. J.; Salmeron, M. B.; Wang, C.; Muller, D. A.; Abruña, H. D.; Yang, P. Operando Methods: A New Era of Electrochemistry. *Curr. Opin. Electrochem.* **2023**, *42*, No. 101403.

(7) Li, J.; Xiong, Q.; Mu, X.; Li, L. Recent Advances in Ammonia Synthesis: From Haber-Bosch Process to External Field Driven Strategies. *ChemSusChem* **2024**, *17*, No. e202301775.

(8) Chen, S.; Chang, X.; Sun, G.; Zhang, T.; Xu, Y.; Wang, Y.; Pei, C.; Gong, J. Propane Dehydrogenation: Catalyst Development, New Chemistry, and Emerging Technologies. *Chem. Soc. Rev.* **2021**, *50*, 3315−3354.

(9) Barelli, L.; Bidini, G.; Gallorini, F.; Servili, S. Hydrogen Production through Sorption-Enhanced Steam Methane Reforming and Membrane Technology: A Review. *Energy (Oxf.)* **2008**, *33*, 554−570.

(10) Suen, N.-T.; Hung, S.-F.; Quan, Q.; Zhang, N.; Xu, Y.-J.; Chen, H. M. Electrocatalysis for the Oxygen Evolution Reaction: Recent Development and Future Perspectives. *Chem. Soc. Rev.* **2017**, *46*, 337−365.

(11) Zhang, B.; Sun, L. Artificial Photosynthesis: Opportunities and Challenges of Molecular Catalysts. *Chem. Soc. Rev.* **2019**, *48*, 2216−2264.

(12) Sundar, K. P.; Kanmani, S. Progression of Photocatalytic Reactors and It's Comparison: A Review. *Chem. Eng. Res. Des.* **2020**, *154*, 135−150.

(13) Bañares, M. A. Operando Methodology: Combination of in Situ Spectroscopy and Simultaneous Activity Measurements under Catalytic Reaction Conditions. *Catal. Today* **2005**, *100*, 71−77.

(14) Guerrero-Pérez, M. O.; Bañares, M. A. Operando Raman Study of Alumina-Supported Sb−V−O Catalyst during Propane Ammoxidation to Acrylonitrile with on-Line Activity Measurement. *Chem. Commun.* **2002**, *12*, 1292−1293.

(15) Bañares, M. A.; Guerrero-Pérez, M. O.; Fierro, J. L. G.; Cortez, G. G. Raman Spectroscopy during Catalytic Operations with On-Line Activity Measurement (Operando Spectroscopy): A Method for Understanding the Active Centres of Cations Supported on Porous Materials. *J. Mater. Chem.* **2002**, *12*, 3337−3342.

(16) Zhu, Y.; Wang, J.; Chu, H.; Chu, Y.-C.; Chen, H. M. *In Situ/Operando* Studies for Designing next-Generation Electrocatalysts. *ACS Energy Lett.* **2020**, *5*, 1281−1291.

(17) Prajapati, A.; Hahn, C.; Weidinger, I. M.; Shi, Y.; Lee, Y.; Alexandrova, A. N.; Thompson, D.; Bare, S. R.; Chen, S.; Yan, S.; Kornienko, N. Best Practices for In-Situ and Operando Techniques within Electrocatalytic Systems. *Nat. Commun.* **2025**, *16*, 2593.

(18) Smeaton, M. A.; Abellan, P.; Spurgeon, S. R.; Unocic, R. R.; Jungjohann, K. L. Tutorial on In Situ and *Operando* (Scanning) Transmission Electron Microscopy for Analysis of Nanoscale Structure−Property Relationships. *ACS Nano* **2024**, *18*, 35091−35103.

(19) Morishita, S.; Ishikawa, R.; Kohno, Y.; Sawada, H.; Shibata, N.; Ikuhara, Y. Attainment of 40.5 Pm Spatial Resolution Using 300 kV Scanning Transmission Electron Microscope Equipped with Fifth-Order Aberration Corrector. *Microscopy* **2018**, *67*, 46−50.

(20) Li, J.; Johnson, G.; Zhang, S.; Su, D. In Situ Transmission Electron Microscopy for Energy Applications. *Joule* **2019**, *3*, 4−8.

(21) Zewail, A. H. 4D Ultrafast Electron Diffraction, Crystallography, and Microscopy. *Annu. Rev. Phys. Chem.* **2006**, *57*, 65−103.

(22) Hwang, S.; Chen, X.; Zhou, G.; Su, D. In Situ Transmission Electron Microscopy on Energy-Related Catalysis. *Adv. Energy Mater.* **2020**, *10*, No. 1902105.

(23) Tang, M.; Yuan, W.; Ou, Y.; Li, G.; You, R.; Li, S.; Yang, H.; Zhang, Z.; Wang, Y. Recent Progresses on Structural Reconstruction of Nanosized Metal Catalysts via Controlled-Atmosphere Transmission Electron Microscopy: A Review. *ACS Catal.* **2020**, *10*, 14419−14450.

(24) Chee, S. W.; Lunkenbein, T.; Schlögl, R.; Roldán Cuenya, B. *Operando* Electron Microscopy of Catalysts: The Missing Cornerstone in Heterogeneous Catalysis Research? *Chem. Rev.* **2023**, *123*, 13374−13418.

(25) Chao, H.-Y.; Venkatraman, K.; Moniri, S.; Jiang, Y.; Tang, X.; Dai, S.; Gao, W.; Miao, J.; Chi, M. *In Situ* and Emerging Transmission Electron Microscopy for Catalysis Research. *Chem. Rev.* **2023**, *123*, 8347−8394.

(26) Yuan, W.; Fang, K.; You, R.; Zhang, Z.; Wang, Y. Toward In Situ Atomistic Design of Catalytic Active Sites via Controlled Atmosphere Transmission Electron Microscopy. *Acc. Mater. Res.* **2023**, *4*, 275−286.

(27) Albrecht, W.; Van Aert, S.; Bals, S. Three-Dimensional Nanoparticle Transformations Captured by an Electron Microscope. *Acc. Chem. Res.* **2021**, *54*, 1189−1199.

(28) Narayan, T. C.; Baldi, A.; Koh, A. L.; Sinclair, R.; Dionne, J. A. Reconstructing Solute-Induced Phase Transformations within Individual Nanocrystals. *Nat. Mater.* **2016**, *15*, 768−774.

(29) Baldi, A.; Narayan, T. C.; Koh, A. L.; Dionne, J. A. In Situ Detection of Hydrogen-Induced Phase Transitions in Individual Palladium Nanocrystals. *Nat. Mater.* **2014**, *13*, 1143−1148.

(30) Pedrazo-Tardajos, A.; Claes, N.; Wang, D.; Sánchez-Iglesias, A.; Nandi, P.; Jenkinson, K.; De Meyer, R.; Liz-Marzán, L. M.; Bals, S. Direct Visualization of Ligands on Gold Nanoparticles in a Liquid Environment. *Nat. Chem.* **2024**, *16*, 1278−1285.

(31) Nilsson Pingel, T.; Jørgensen, M.; Yankovich, A. B.; Grönbeck, H.; Olsson, E. Influence of Atomic Site-Specific Strain on Catalytic Activity of Supported Nanoparticles. *Nat. Commun.* **2018**, *9*, 2722.

(32) Tao, F. F.; Crozier, P. A. Atomic-Scale Observations of Catalyst Structures under Reaction Conditions and during Catalysis. *Chem. Rev.* **2016**, *116*, 3487−3539.

(33) Chenna, S.; Banerjee, R.; Crozier, P. A. Atomic-Scale Observation of the Ni Activation Process for Partial Oxidation of Methane Using In Situ Environmental TEM. *ChemCatChem.* **2011**, *3*, 1051−1059.

(34) Jiang, Y.; Lim, A. M. H.; Yan, H.; Zeng, H. C.; Mirsaidov, U. Phase Segregation in PdCu Alloy Nanoparticles During CO Oxidation Reaction at Atmospheric Pressure. *Adv. Sci.* **2023**, *10*, No. 2302663.

(35) Ghosh, T.; Liu, X.; Sun, W.; Chen, M.; Liu, Y.; Li, Y.; Mirsaidov, U. Revealing the Origin of Low-Temperature Activity of Ni−Rh Nanostructures during CO Oxidation Reaction with Operando TEM. *Adv. Sci.* **2022**, *9*, No. 2105599.

(36) Jiang, Y.; Wong, Z. M.; Yan, H.; Tan, T. L.; Mirsaidov, U. Revealing Multistep Phase Separation in Metal Alloy Nanoparticles with *In Situ* Transmission Electron Microscopy. *ACS Nano* **2025**, *19*, 3886−3894.

(37) Altantzis, T.; Lobato, I.; De Backer, A.; Béché, A.; Zhang, Y.; Basak, S.; Porcu, M.; Xu, Q.; Sánchez-Iglesias, A.; Liz-Marzán, L. M.; Van Tendeloo, G.; Van Aert, S.; Bals, S. Three-Dimensional Quantification of the Facet Evolution of Pt Nanoparticles in a Variable Gaseous Environment. *Nano Lett.* **2019**, *19*, 477−481.

(38) Yoshida, H.; Kuwauchi, Y.; Jinschek, J. R.; Sun, K.; Tanaka, S.; Kohyama, M.; Shimada, S.; Haruta, M.; Takeda, S. Visualizing Gas Molecules Interacting with Supported Nanoparticulate Catalysts at Reaction Conditions. *Science* **2012**, *335*, 317−319.

(39) Avanesian, T.; Dai, S.; Kale, M. J.; Graham, G. W.; Pan, X.; Christopher, P. Quantitative and Atomic-Scale View of CO-Induced Pt Nanoparticle Surface Reconstruction at Saturation Coverage via DFT Calculations Coupled with *in Situ* TEM and IR. *J. Am. Chem. Soc.* **2017**, *139*, 4551−4558.

(40) Dai, S.; Hou, Y.; Onoue, M.; Zhang, S.; Gao, W.; Yan, X.; Graham, G. W.; Wu, R.; Pan, X. Revealing Surface Elemental Composition and Dynamic Processes Involved in Facet-Dependent Oxidation of Pt_3Co Nanoparticles via *in Situ* Transmission Electron Microscopy. *Nano Lett.* **2017**, *17*, 4683−4688.

(41) Zhang, X.; Han, S.; Zhu, B.; Zhang, G.; Li, X.; Gao, Y.; Wu, Z.; Yang, B.; Liu, Y.; Baaziz, W.; Ersen, O.; Gu, M.; Miller, J. T.; Liu, W. Reversible Loss of Core−Shell Structure for Ni−Au Bimetallic Nanoparticles during CO_2 Hydrogenation. *Nat. Catal.* **2020**, *3*, 411−417.

(42) Foucher, A. C.; Yang, S.; Rosen, D. J.; Huang, R.; Pyo, J. B.; Kwon, O.; Owen, C. J.; Sanchez, D. F.; Sadykov, I. I.; Grolimund, D.; Kozinsky, B.; Frenkel, A. I.; Gorte, R. J.; Murray, C. B.; Stach, E. A. Synthesis and Characterization of Stable Cu-Pt Nanoparticles under Reductive and Oxidative Conditions. *J. Am. Chem. Soc.* **2023**, *145*, 5410−5421.

(43) Simonsen, S. B.; Chorkendorff, I.; Dahl, S.; Skoglundh, M.; Sehested, J.; Helveg, S. Direct Observations of Oxygen-Induced Platinum Nanoparticle Ripening Studied by In Situ TEM. *J. Am. Chem. Soc.* **2010**, *132*, 7968−7975.

(44) Yuan, W.; Zhang, D.; Ou, Y.; Fang, K.; Zhu, B.; Yang, H.; Hansen, T. W.; Wagner, J. B.; Zhang, Z.; Gao, Y.; Wang, Y. Direct In Situ TEM Visualization and Insight into the Facet-Dependent Sintering Behaviors of Gold on TiO_2. *Angew. Chem., Int. Ed. Engl.* **2018**, *57*, 16827−16831.

(45) Beck, A.; Huang, X.; Artiglia, L.; Zabilskiy, M.; Wang, X.; Rzepka, P.; Palagin, D.; Willinger, M.-G.; Van Bokhoven, J. A. The Dynamics of Overlayer Formation on Catalyst Nanoparticles and Strong Metal-Support Interaction. *Nat. Commun.* **2020**, *11*, 3220.

(46) Liu, S.; Xu, W.; Niu, Y.; Zhang, B.; Zheng, L.; Liu, W.; Li, L.; Wang, J. Ultrastable Au Nanoparticles on Titania through an Encapsulation Strategy under Oxidative Atmosphere. *Nat. Commun.* **2019**, *10*, 5790.

(47) Liu, L.; Zakharov, D. N.; Arenal, R.; Concepcion, P.; Stach, E. A.; Corma, A. Evolution and Stabilization of Subnanometric Metal

Species in Confined Space by in Situ TEM. *Nat. Commun.* **2018**, *9*, 574.

(48) Tang, H.; Su, Y.; Zhang, B.; Lee, A. F.; Isaacs, M. A.; Wilson, K.; Li, L.; Ren, Y.; Huang, J.; Haruta, M.; Qiao, B.; Liu, X.; Jin, C.; Su, D.; Wang, J.; Zhang, T. Classical Strong Metal−Support Interactions between Gold Nanoparticles and Titanium Dioxide. *Sci. Adv.* **2017**, *3*, No. e1700231.

(49) Matsubu, J. C.; Zhang, S.; DeRita, L.; Marinkovic, N. S.; Chen, J. G.; Graham, G. W.; Pan, X.; Christopher, P. Adsorbate-Mediated Strong Metal−Support Interactions in Oxide-Supported Rh Catalysts. *Nat. Chem.* **2017**, *9*, 120−127.

(50) Frey, H.; Beck, A.; Huang, X.; Van Bokhoven, J. A.; Willinger, M. G. Dynamic Interplay between Metal Nanoparticles and Oxide Support under Redox Conditions. *Science* **2022**, *376*, 982−987.

(51) Lee, S.; Gadelrab, K.; Cheng, L.; Braaten, J. P.; Wu, H.; Ross, F. M. Simultaneous 2D Projection and 3D Topographic Imaging of Gas-Dependent Dynamics of Catalytic Nanoparticles. *ACS Nano* **2024**, *18*, 21258−21267.

(52) Ross, F. M. *Liquid Cell Electron Microscopy*; Cambridge University Press: Cambridge, England, 2017.

(53) Ross, F. M. Opportunities and Challenges in Liquid Cell Electron Microscopy. *Science* **2015**, *350*, No. aaa9886.

(54) Fratarcangeli, M.; Vigil, S. A.; Moreno-Hernandez, I. A. Understanding Electrochemical Degradation via Liquid Phase Transmission Electron Microscopy. *J. Phys. Chem. C Nanomater. Interfaces* **2025**, *129*, 7612−7624.

(55) Yuk, J. M.; Park, J.; Ercius, P.; Kim, K.; Hellebusch, D. J.; Crommie, M. F.; Lee, J. Y.; Zettl, A.; Alivisatos, A. P. High-Resolution EM of Colloidal Nanocrystal Growth Using Graphene Liquid Cells. *Science* **2012**, *336*, 61−64.

(56) Yang, J.; Alam, S. B.; Yu, L.; Chan, E.; Zheng, H. Dynamic Behavior of Nanoscale Liquids in Graphene Liquid Cells Revealed by in Situ Transmission Electron Microscopy. *Micron* **2019**, *116*, 22−29.

(57) de Jonge, N.; Ross, F. M. Electron Microscopy of Specimens in Liquid. *Nat. Nanotechnol.* **2011**, *6*, 695−704.

(58) Williamson, M. J.; Tromp, R. M.; Vereecken, P. M.; Hull, R.; Ross, F. M. Dynamic Microscopy of Nanoscale Cluster Growth at the Solid-Liquid Interface. *Nat. Mater.* **2003**, *2*, 532−536.

(59) Chee, S. W.; Lunkenbein, T.; Schlögl, R.; Cuenya, B. R. In Situ and Operando Electron Microscopy in Heterogeneous Catalysis—Insights into Multi-Scale Chemical Dynamics. *J. Phys.: Condens. Matter* **2021**, *33*, No. 153001.

(60) Ghosh, T.; Arce-Ramos, J. M.; Li, W.-Q.; Yan, H.; Chee, S. W.; Genest, A.; Mirsaidov, U. Periodic Structural Changes in Pd Nanoparticles during Oscillatory CO Oxidation Reaction. *Nat. Commun.* **2022**, *13*, 6176.

(61) Yoon, A.; Bai, L.; Yang, F.; Franco, F.; Zhan, C.; Rüscher, M.; Timoshenko, J.; Pratsch, C.; Werner, S.; Jeon, H. S.; Monteiro, M. C. D. O.; Chee, S. W.; Roldan Cuenya, B. Revealing Catalyst Restructuring and Composition during Nitrate Electroreduction through Correlated Operando Microscopy and Spectroscopy. *Nat. Mater.* **2025**, *24*, 762−769.

(62) Lee, S.; Fleuren, N. F. J.; Pinkowitz, A.; Ross, F. M. Patterned Electrochemical Deposition through Local Heating of Electrodes. *J. Electrochem. Soc.* **2025**, *172*, No. 022506.

(63) Tan, S. F.; Reidy, K.; Lee, S.; Klein, J.; Schneider, N. M.; Lee, H. Y.; Ross, F. M. Multilayer Graphene—A Promising Electrode Material in Liquid Cell Electrochemistry. *Adv. Funct. Mater.* **2021**, *31*, No. 2104628.

(64) Beermann, V.; Holtz, M. E.; Padgett, E.; de Araujo, J. F.; Muller, D. A.; Strasser, P. Real-Time Imaging of Activation and Degradation of Carbon Supported Octahedral Pt−Ni Alloy Fuel Cell Catalysts at the Nanoscale Using*in Situ*Electrochemical Liquid Cell STEM. *Energy Environ. Sci.* **2019**, *12*, 2476−2485.

(65) Zhang, Q.; Song, Z.; Sun, X.; Liu, Y.; Wan, J.; Betzler, S. B.; Zheng, Q.; Shangguan, J.; Bustillo, K. C.; Ercius, P.; Narang, P.; Huang, Y.; Zheng, H. Atomic Dynamics of Electrified Solid-Liquid Interfaces in Liquid-Cell TEM. *Nature* **2024**, *630*, 643−647.

(66) Kim, S.; Kwag, J.; Lee, M.; Kang, S.; Kim, D.; Oh, J.-G.; Heo, Y.-J.; Ryu, J.; Park, J. Unraveling Serial Degradation Pathways of Supported Catalysts through Reliable Electrochemical Liquid-Cell TEM Analysis. *J. Am. Chem. Soc.* **2025**, *147*, 181−191.

(67) Zeng, L.; Holmér, J.; Dhall, R.; Gammer, C.; Minor, A. M.; Olsson, E. Tuning Hole Mobility of Individual P-Doped GaAs Nanowires by Uniaxial Tensile Stress. *Nano Lett.* **2021**, *21*, 3894−3900.

(68) Yang, Y.; Louisia, S.; Yu, S.; Jin, J.; Roh, I.; Chen, C.; Fonseca Guzman, M. V.; Feijóo, J.; Chen, P.-C.; Wang, H.; Pollock, C. J.; Huang, X.; Shao, Y.-T.; Wang, C.; Muller, D. A.; Abruña, H. D.; Yang, P. Operando Studies Reveal Active Cu Nanograins for CO_2 Electroreduction. *Nature* **2023**, *614*, 262−269.

(69) Fritsch, B.; Lee, S.; Körner, A.; Schneider, N. M.; Ross, F. M.; Hutzler, A. The Influence of Ionizing Radiation on Quantification for In Situ and Operando Liquid-Phase Electron Microscopy. *Adv. Mater.* **2025**, *37*, No. 2415728.

(70) Moreno-Hernandez, I. A.; Crook, M. F.; Ondry, J. C.; Alivisatos, A. P. Redox Mediated Control of Electrochemical Potential in Liquid Cell Electron Microscopy. *J. Am. Chem. Soc.* **2021**, *143*, 12082−12089.

(71) Lee, S.; Schneider, N. M.; Tan, S. F.; Ross, F. M. Temperature Dependent Nanochemistry and Growth Kinetics Using Liquid Cell Transmission Electron Microscopy. *ACS Nano* **2023**, *17*, 5609−5619.

(72) Lee, S.; Watanabe, T.; Ross, F. M.; Park, J. H. Temperature Dependent Growth Kinetics of Pd Nanocrystals: Insights from Liquid Cell Transmission Electron Microscopy. *Small* **2024**, *20*, No. 2403969.

(73) Khelfa, A.; Nelayah, J.; Amara, H.; Wang, G.; Ricolleau, C.; Alloyeau, D. Quantitative in Situ Visualization of Thermal Effects on the Formation of Gold Nanocrystals in Solution. *Adv. Mater.* **2021**, *33*, No. 2102514.

(74) Li, D.; Chen, Q.; Chun, J.; Fichthorn, K.; De Yoreo, J.; Zheng, H. Nanoparticle Assembly and Oriented Attachment: Correlating Controlling Factors to the Resulting Structures. *Chem. Rev.* **2023**, *123*, 3127−3159.

(75) Wan, J.; Zhang, Q.; Liu, E.; Chen, Y.; Zheng, J.; Ren, A.; Drisdell, W. S.; Zheng, H. In-Situ/Operando Study of Cu-Based Nanocatalysts for CO2 Electroreduction Using Electrochemical Liquid Cell TEM. *Front. Chem.* **2025**, *13*, No. 1525245.

(76) Yang, J.; Zeng, Z.; Kang, J.; Betzler, S.; Czarnik, C.; Zhang, X.; Ophus, C.; Yu, C.; Bustillo, K.; Pan, M.; Qiu, J.; Wang, L.-W.; Zheng, H. Formation of Two-Dimensional Transition Metal Oxide Nanosheets with Nanoparticles as Intermediates. *Nat. Mater.* **2019**, *18*, 970−976.

(77) Kim, S.; Briega-Martos, V.; Liu, S.; Je, K.; Shi, C.; Stephens, K. M.; Zeltmann, S. E.; Zhang, Z.; Guzman-Soriano, R.; Li, W.; Jiang, J.; Choi, J.; Negash, Y. J.; Walden, F. S., 2nd; Marthe, N. L., Jr.; Wellborn, P. S.; Guo, Y.; Damiano, J.; Han, Y.; Thiede, E. H.; Yang, Y. Operando Heating and Cooling Electrochemical 4D-STEM Probing Nanoscale Dynamics at Solid-Liquid Interfaces. *J. Am. Chem. Soc.* **2025**, *147*, 23654−23671.

(78) Tan, S. F.; Reidy, K.; Klein, J.; Pinkowitz, A.; Wang, B.; Ross, F. M. Real-Time Imaging of Nanoscale Electrochemical Ni Etching under Thermal Conditions. *Chem. Sci.* **2021**, *12*, 5259−5268.

(79) Swearer, D. F.; Bourgeois, B. B.; Angell, D. K.; Dionne, J. A. Advancing Plasmon-Induced Selectivity in Chemical Transformations with Optically Coupled Transmission Electron Microscopy. *Acc. Chem. Res.* **2021**, *54*, 3632−3642.

(80) Vadai, M.; Angell, D. K.; Hayee, F.; Sytwu, K.; Dionne, J. A. In-Situ Observation of Plasmon-Controlled Photocatalytic Dehydrogenation of Individual Palladium Nanoparticles. *Nat. Commun.* **2018**, *9*, 4658.

(81) Sytwu, K.; Vadai, M.; Hayee, F.; Angell, D. K.; Dai, A.; Dixon, J.; Dionne, J. A. Driving Energetically Unfavorable Dehydrogenation Dynamics with Plasmonics. *Science* **2021**, *371*, 280−283.

(82) Krivanek, O. L.; Lovejoy, T. C.; Dellby, N.; Aoki, T.; Carpenter, R. W.; Rez, P.; Soignard, E.; Zhu, J.; Batson, P. E.; Lagos,

M. J.; Egerton, R. F.; Crozier, P. A. Vibrational Spectroscopy in the Electron Microscope. *Nature* **2014**, *514*, 209−212.

(83) Chen, P.-C.; Chen, C.; Yang, Y.; Maulana, A. L.; Jin, J.; Feijoo, J.; Yang, P. Chemical and Structural Evolution of AgCu Catalysts in Electrochemical CO_2 Reduction. *J. Am. Chem. Soc.* **2023**, *145*, 10116−10125.

(84) Crozier, P. A.; Aoki, T.; Liu, Q.; Zhang, L. Detection and Characterization of OH Vibrational Modes Using High Energy Resolution EELS. *Microanal* **2015**, *21*, 1473−1474.

(85) Singh, J.; Lamberti, C.; van Bokhoven, J. A. Advanced X-Ray Absorption and Emission Spectroscopy: In Situ Catalytic Studies. *Chem. Soc. Rev.* **2010**, *39*, 4754−4766.

(86) Timoshenko, J.; Roldan Cuenya, B. In Situ/Operando Electrocatalyst Characterization by X-Ray Absorption Spectroscopy. *Chem. Rev.* **2021**, *121*, 882−961.

(87) Li, X.; Wang, H.-Y.; Yang, H.; Cai, W.; Liu, S.; Liu, B. In Situ/Operando Characterization Techniques to Probe the Electrochemical Reactions for Energy Conversion. *Small Methods* **2018**, *2*, No. 1700395.

(88) Tsoukalou, A.; Abdala, P. M.; Stoian, D.; Huang, X.; Willinger, M.-G.; Fedorov, A.; Müller, C. R. Structural Evolution and Dynamics of an In_2O_3 Catalyst for CO_2 Hydrogenation to Methanol: An Operando XAS-XRD and in Situ TEM Study. *J. Am. Chem. Soc.* **2019**, *141*, 13497−13505.

(89) Yang, Y.; Wang, Y.; Xiong, Y.; Huang, X.; Shen, L.; Huang, R.; Wang, H.; Pastore, J. P.; Yu, S.-H.; Xiao, L.; Brock, J. D.; Zhuang, L.; Abruña, H. D. *In Situ* X-Ray Absorption Spectroscopy of a Synergistic Co-Mn Oxide Catalyst for the Oxygen Reduction Reaction. *J. Am. Chem. Soc.* **2019**, *141*, 1463−1466.

(90) Yang, Y.; Xiong, Y.; Zeng, R.; Lu, X.; Krumov, M.; Huang, X.; Xu, W.; Wang, H.; DiSalvo, F. J.; Brock, J. D.; Muller, D. A.; Abruña, H. D. *Operando*Methods in Electrocatalysis. *ACS Catal.* **2021**, *11*, 1136−1178.

(91) Fabbri, E.; Abbott, D. F.; Nachtegaal, M.; Schmidt, T. J. Operando X-Ray Absorption Spectroscopy: A Powerful Tool toward Water Splitting Catalyst Development. *Curr. Opin. Electrochem.* **2017**, *5*, 20−26.

(92) van Oversteeg, C. H. M.; Doan, H. Q.; de Groot, F. M. F.; Cuk, T. In Situ X-Ray Absorption Spectroscopy of Transition Metal Based Water Oxidation Catalysts. *Chem. Soc. Rev.* **2017**, *46*, 102−125.

(93) Xie, Y.; Sun, Y.; Tao, H.; Wang, X.; Wu, J.; Ma, K.; Wang, L.; Kang, Z.; Zhang, Y. In Situ Investigation on Life-time Dynamic Structure−Performance Correlation toward Electrocatalyst Service Behavior in Water Splitting. *Adv. Funct. Mater.* **2022**, *32*, No. 2111777.

(94) Wang, B.; Chu, S.; Zheng, L.; Li, X.; Zhang, J.; Zhang, F. Application of X-Ray Absorption Spectroscopy in Electrocatalytic Water Splitting and CO_2 Reduction. *Small Sci.* **2021**, *1*, No. 2100023.

(95) Li, X.; Wang, S.; Li, L.; Sun, Y.; Xie, Y. Progress and Perspective for in Situ Studies of CO_2 Reduction. *J. Am. Chem. Soc.* **2020**, *142*, 9567−9581.

(96) Wang, J.; Tan, H.-Y.; Zhu, Y.; Chu, H.; Chen, H. M. Linking the Dynamic Chemical State of Catalysts with the Product Profile of Electrocatalytic CO_2 Reduction. *Angew. Chem., Int. Ed. Engl.* **2021**, *60*, 17254−17267.

(97) Zou, Y.; Wang, S. An Investigation of Active Sites for Electrochemical CO_2 Reduction Reactions: From in Situ Characterization to Rational Design. *Adv. Sci.* **2021**, *8*, No. 2003579.

(98) Wu, X.; Guo, Y.; Sun, Z.; Xie, F.; Guan, D.; Dai, J.; Yu, F.; Hu, Z.; Huang, Y.-C.; Pao, C.-W.; Chen, J.-L.; Zhou, W.; Shao, Z. Fast Operando Spectroscopy Tracking in Situ Generation of Rich Defects in Silver Nanocrystals for Highly Selective Electrochemical CO_2 Reduction. *Nat. Commun.* **2021**, *12*, 660.

(99) Velasco-Velez, J.-J.; Mom, R. V.; Sandoval-Diaz, L.-E.; Falling, L. J.; Chuang, C.-H.; Gao, D.; Jones, T. E.; Zhu, Q.; Arrigo, R.; Roldan Cuenya, B.; Knop-Gericke, A.; Lunkenbein, T.; Schlögl, R. Revealing the Active Phase of Copper during the Electroreduction of CO_2 in Aqueous Electrolyte by Correlating in Situ X-Ray Spectroscopy and in Situ Electron Microscopy. *ACS Energy Lett.* **2020**, *5*, 2106−2111.

(100) Yang, Y.; Shi, C.; Feijóo, J.; Jin, J.; Chen, C.; Han, Y.; Yang, P. Dynamic Evolution of Copper Nanowires during CO_2 Reduction Probed by Operando Electrochemical 4D-STEM and X-Ray Spectroscopy. *J. Am. Chem. Soc.* **2024**, *146*, 23398−23405.

(101) Abbott, D. F.; Lebedev, D.; Waltar, K.; Povia, M.; Nachtegaal, M.; Fabbri, E.; Copéret, C.; Schmidt, T. J. Iridium Oxide for the Oxygen Evolution Reaction: Correlation between Particle Size, Morphology, and the Surface Hydroxo Layer from Operando XAS. *Chem. Mater.* **2016**, *28*, 6591−6604.

(102) Diklić, N.; Clark, A. H.; Herranz, J.; Diercks, J. S.; Aegerter, D.; Nachtegaal, M.; Beard, A.; Schmidt, T. J. Potential Pitfalls in the *Operando* XAS Study of Oxygen Evolution Electrocatalysts. *ACS Energy Lett.* **2022**, *7*, 1735−1740.

(103) Zuo, S.; Wu, Z.; Zhang, H.; Lou, X. W. Operando Monitoring and Deciphering the Structural Evolution in Oxygen Evolution Electrocatalysis. *Adv. Energy Mater.* **2022**, *12*, No. 2103383.

(104) Favaro, M.; Drisdell, W. S.; Marcus, M. A.; Gregoire, J. M.; Crumlin, E. J.; Haber, J. A.; Yano, J. An Operando Investigation of $(Ni-Fe-Co-Ce)O_x$ System as Highly Efficient Electrocatalyst for Oxygen Evolution Reaction. *ACS Catal.* **2017**, *7*, 1248−1258.

(105) Czioska, S.; Boubnov, A.; Escalera-López, D.; Geppert, J.; Zagalskaya, A.; Röse, P.; Saraçi, E.; Alexandrov, V.; Krewer, U.; Cherevko, S.; Grunwaldt, J.-D. Increased Ir−Ir Interaction in Iridium Oxide during the Oxygen Evolution Reaction at High Potentials Probed by Operando Spectroscopy. *ACS Catal.* **2021**, *11*, 10043−10057.

(106) Deka, N.; Jones, T. E.; Falling, L. J.; Sandoval-Diaz, L.-E.; Lunkenbein, T.; Velasco-Velez, J.-J.; Chan, T.-S.; Chuang, C.-H.; Knop-Gericke, A.; Mom, R. V. On the Operando Structure of Ruthenium Oxides during the Oxygen Evolution Reaction in Acidic Media. *ACS Catal.* **2023**, *13*, 7488−7498.

(107) Nong, H. N.; Falling, L. J.; Bergmann, A.; Klingenhof, M.; Tran, H. P.; Spöri, C.; Mom, R.; Timoshenko, J.; Zichittella, G.; Knop-Gericke, A.; Piccinin, S.; Pérez-Ramírez, J.; Cuenya, B. R.; Schlögl, R.; Strasser, P.; Teschner, D.; Jones, T. E. Key Role of Chemistry versus Bias in Electrocatalytic Oxygen Evolution. *Nature* **2020**, *587*, 408−413.

(108) Gao, J.; Xu, C.-Q.; Hung, S.-F.; Liu, W.; Cai, W.; Zeng, Z.; Jia, C.; Chen, H. M.; Xiao, H.; Li, J.; Huang, Y.; Liu, B. Breaking Long-Range Order in Iridium Oxide by Alkali Ion for Efficient Water Oxidation. *J. Am. Chem. Soc.* **2019**, *141*, 3014−3023.

(109) Danilovic, N.; Subbaraman, R.; Chang, K.-C.; Chang, S. H.; Kang, Y. J.; Snyder, J.; Paulikas, A. P.; Strmcnik, D.; Kim, Y.-T.; Myers, D.; Stamenkovic, V. R.; Markovic, N. M. Activity−Stability Trends for the Oxygen Evolution Reaction on Monometallic Oxides in Acidic Environments. *J. Phys. Chem. Lett.* **2014**, *5*, 2474−2478.

(110) Kim, M.; Lee, B.; Ju, H.; Lee, S. W.; Kim, J. Reducing the Barrier Energy of Self-Reconstruction for Anchored Cobalt Nanoparticles as Highly Active Oxygen Evolution Electrocatalyst. *Adv. Mater.* **2019**, *31*, No. 1901977.

(111) Deng, Y.; Yeo, B. S. Characterization of Electrocatalytic Water Splitting and CO_2Reduction Reactions Using in Situ/Operando Raman Spectroscopy. *ACS Catal.* **2017**, *7*, 7873−7889.

(112) Begildayeva, T.; Theerthagiri, J.; Lee, S. J.; Yu, Y.; Choi, M. Y. Unraveling the Synergy of Anion Modulation on Co Electrocatalysts by Pulsed Laser for Water Splitting: Intermediate Capturing by in Situ/Operando Raman Studies. *Small* **2022**, *18*, No. 2204309.

(113) Yao, K.; Li, J.; Wang, H.; Lu, R.; Yang, X.; Luo, M.; Wang, N.; Wang, Z.; Liu, C.; Jing, T.; Chen, S.; Cortés, E.; Maier, S. A.; Zhang, S.; Li, T.; Yu, Y.; Liu, Y.; Kang, X.; Liang, H. Mechanistic Insights into OC−COH Coupling in CO_2 Electroreduction on Fragmented Copper. *J. Am. Chem. Soc.* **2022**, *144*, 14005−14011.

(114) Frontiera, R. R.; Henry, A.-I.; Gruenke, N. L.; Van Duyne, R. P. Surface-Enhanced Femtosecond Stimulated Raman Spectroscopy. *J. Phys. Chem. Lett.* **2011**, *2*, 1199−1203.

(115) Brooks, J. L.; Warkentin, C. L.; Chulhai, D. V.; Goodpaster, J. D.; Frontiera, R. R. Plasmon-Mediated Intramolecular Methyl

Migration with Nanoscale Spatial Control. *ACS Nano* **2020**, *14*, 17194−17202.
(116) Wilson, A. J.; Jain, P. K. Structural Dynamics of the Oxygen-Evolving Complex of Photosystem II in Water-Splitting Action. *J. Am. Chem. Soc.* **2018**, *140*, 5853−5859.
(117) Keller, E. L.; Frontiera, R. R. Ultrafast Nanoscale Raman Thermometry Proves Heating Is Not a Primary Mechanism for Plasmon-Driven Photocatalysis. *ACS Nano* **2018**, *12*, 5848−5855.
(118) Tagliabue, G.; DuChene, J. S.; Abdellah, M.; Habib, A.; Gosztola, D. J.; Hattori, Y.; Cheng, W.-H.; Zheng, K.; Canton, S. E.; Sundararaman, R.; Sá, J.; Atwater, H. A. Ultrafast Hot-Hole Injection Modifies Hot-Electron Dynamics in Au/p-GaN Heterostructures. *Nat. Mater.* **2020**, *19*, 1312−1318.
(119) Huang, T.-X.; Cong, X.; Wu, S.-S.; Wu, J.-B.; Bao, Y.-F.; Cao, M.-F.; Wu, L.; Lin, M.-L.; Wang, X.; Tan, P.-H.; Ren, B. Visualizing the Structural Evolution of Individual Active Sites in MoS_2 during Electrocatalytic Hydrogen Evolution Reaction. *Nat. Catal.* **2024**, *7*, 646−654.
(120) Nørskov, J. K.; Rossmeisl, J.; Logadottir, A.; Lindqvist, L.; Kitchin, J. R.; Bligaard, T.; Jónsson, H. Origin of the Overpotential for Oxygen Reduction at a Fuel-Cell Cathode. *J. Phys. Chem. B* **2004**, *108*, 17886−17892.
(121) Nørskov, J. K.; Bligaard, T.; Logadottir, A.; Kitchin, J. R.; Chen, J. G.; Pandelov, S.; Stimming, U. Trends in the Exchange Current for Hydrogen Evolution. *J. Electrochem. Soc.* **2005**, *152*, J23.
(122) Man, I. C.; Su, H.; Calle-Vallejo, F.; Hansen, H. A.; Martínez, J. I.; Inoglu, N. G.; Kitchin, J.; Jaramillo, T. F.; Nørskov, J. K.; Rossmeisl, J. Universality in Oxygen Evolution Electrocatalysis on Oxide Surfaces. *ChemCatChem* **2011**, *3*, 1159−1165.
(123) Greeley, J.; Jaramillo, T. F.; Bonde, J.; Chorkendorff, I.; Nørskov, J. K. Computational High-Throughput Screening of Electrocatalytic Materials for Hydrogen Evolution. *Nat. Mater.* **2006**, *5*, 909−913.
(124) Cheng, D.; Nguyen, K.-L. C.; Sumaria, V.; Wei, Z.; Zhang, Z.; Gee, W.; Li, Y.; Morales-Guio, C. G.; Heyde, M.; Roldan Cuenya, B.; Alexandrova, A. N.; Sautet, P. Structure Sensitivity and Catalyst Restructuring for CO_2 Electro-Reduction on Copper. *Nat. Commun.* **2025**, *16*, 4064.
(125) Zhang, Z.; Zandkarimi, B.; Alexandrova, A. N. Ensembles of Metastable States Govern Heterogeneous Catalysis on Dynamic Interfaces. *Acc. Chem. Res.* **2020**, *53*, 447−458.
(126) Guan, H.; Harris, C.; Sun, S. Metal-Ligand Interactions and Their Roles in Controlling Nanoparticle Formation and Functions. *Acc. Chem. Res.* **2023**, *56*, 1591−1601.
(127) Reuter, K.; Plaisance, C. P.; Oberhofer, H.; Andersen, M. Perspective: On the Active Site Model in Computational Catalyst Screening. *J. Chem. Phys.* **2017**, *146*, No. 040901.
(128) Diesen, E.; Dudzinski, A. M.; Reuter, K.; Bukas, V. J. Origin of Electrocatalytic Selectivity during the Oxygen Reduction Reaction on Au(111). *ACS Catal.* **2025**, *15*, 5403−5411.
(129) Liu, H.-Z.; Shu, X.-X.; Huang, M.; Wu, B.-B.; Chen, J.-J.; Wang, X.-S.; Li, H.-L.; Yu, H.-Q. Tailoring D-Band Center of High-Valent Metal-Oxo Species for Pollutant Removal via Complete Polymerization. *Nat. Commun.* **2024**, *15*, 2327.
(130) Hu, Q.; Gao, K.; Wang, X.; Zheng, H.; Cao, J.; Mi, L.; Huo, Q.; Yang, H.; Liu, J.; He, C. Subnanometric Ru Clusters with Upshifted D Band Center Improve Performance for Alkaline Hydrogen Evolution Reaction. *Nat. Commun.* **2022**, *13*, 3958.
(131) Kim, Y.; Collinge, G.; Lee, M.-S.; Khivantsev, K.; Cho, S. J.; Glezakou, V.-A.; Rousseau, R.; Szanyi, J.; Kwak, J. H. Surface Density Dependent Catalytic Activity of Single Palladium Atoms Supported on Ceria. *Angew. Chem., Int. Ed. Engl.* **2021**, *60*, 22769−22775.
(132) Chen, L.; Allec, S. I.; Nguyen, M.-T.; Kovarik, L.; Hoffman, A. S.; Hong, J.; Meira, D.; Shi, H.; Bare, S. R.; Glezakou, V.-A.; Rousseau, R.; Szanyi, J. Dynamic Evolution of Palladium Single Atoms on Anatase Titania Support Determines the Reverse Water-Gas Shift Activity. *J. Am. Chem. Soc.* **2023**, *145*, 10847−10860.
(133) Bruix, A.; Füchtbauer, H. G.; Tuxen, A. K.; Walton, A. S.; Andersen, M.; Porsgaard, S.; Besenbacher, F.; Hammer, B.; Lauritsen, J. V. In Situ Detection of Active Edge Sites in Single-Layer MoS_2 Catalysts. *ACS Nano* **2015**, *9*, 9322−9330.
(134) Adamsen, K. C.; Kolsbjerg, E. L.; Koust, S.; Lammich, L.; Hammer, B.; Wendt, S.; Lauritsen, J. V. NH_3 on Anatase $TiO_2(101)$: Diffusion Mechanisms and the Effect of Intermolecular Repulsion. *Phys. Rev. Mater.* **2020**, *4*, No. 121601.
(135) Beinik, I.; Bruix, A.; Li, Z.; Adamsen, K. C.; Koust, S.; Hammer, B.; Wendt, S.; Lauritsen, J. V. Water Dissociation and Hydroxyl Ordering on Anatase $TiO_2(001)$-(1×4). *Phys. Rev. Lett.* **2018**, *121*, No. 206003.
(136) Vara, M.; Roling, L. T.; Wang, X.; Elnabawy, A. O.; Hood, Z. D.; Chi, M.; Mavrikakis, M.; Xia, Y. Understanding the Thermal Stability of Palladium−Platinum Core−Shell Nanocrystals by *In Situ* Transmission Electron Microscopy and Density Functional Theory. *ACS Nano* **2017**, *11*, 4571−4581.
(137) Liu, H.; An, W.; Li, Y.; Frenkel, A. I.; Sasaki, K.; Koenigsmann, C.; Su, D.; Anderson, R. M.; Crooks, R. M.; Adzic, R. R.; Liu, P.; Wong, S. S. In Situ Probing of the Active Site Geometry of Ultrathin Nanowires for the Oxygen Reduction Reaction. *J. Am. Chem. Soc.* **2015**, *137*, 12597−12609.
(138) Friebel, D.; Viswanathan, V.; Miller, D. J.; Anniyev, T.; Ogasawara, H.; Larsen, A. H.; O'Grady, C. P.; Nørskov, J. K.; Nilsson, A. Balance of Nanostructure and Bimetallic Interactions in Pt Model Fuel Cell Catalysts: In Situ XAS and DFT Study. *J. Am. Chem. Soc.* **2012**, *134*, 9664−9671.
(139) Zhang, R.; Ma, H.; Han, S.; Wu, Z.; Zhou, X.; Chen, Z.; Liu, J.; Xiao, Y.; Chen, W.; Loh, K. P. Dynamically Stable Cu^0 $Cu^{\delta+}$ Pair Sites Based on In Situ-Exsolved Cu Nanoclusters on $CaCO_3$ for Efficient CO_2 Electroreduction. *Angew. Chem., Int. Ed.* **2025**, *64*, No. e202421860.
(140) Su, X.; Jiang, Z.; Zhou, J.; Liu, H.; Zhou, D.; Shang, H.; Ni, X.; Peng, Z.; Yang, F.; Chen, W.; Qi, Z.; Wang, D.; Wang, Y. Complementary Operando Spectroscopy Identification of in-Situ Generated Metastable Charge-Asymmetry Cu_2-CuN_3 Clusters for CO_2 Reduction to Ethanol. *Nat. Commun.* **2022**, *13*, 1322.
(141) Seger, B.; Kastlunger, G.; Bagger, A.; Scott, S. A Perspective on the Reaction Mechanisms of CO_2 Electrolysis. *ACS Energy Lett.* **2025**, *10*, 2212−2227.
(142) Ren, X.; Zhao, J.; Li, X.; Shao, J.; Pan, B.; Salamé, A.; Boutin, E.; Groizard, T.; Wang, S.; Ding, J.; Zhang, X.; Huang, W.-Y.; Zeng, W.-J.; Liu, C.; Li, Y.; Hung, S.-F.; Huang, Y.; Robert, M.; Liu, B. In-Situ Spectroscopic Probe of the Intrinsic Structure Feature of Single-Atom Center in Electrochemical CO/CO_2 Reduction to Methanol. *Nat. Commun.* **2023**, *14*, 3401.
(143) Zhong, H.-L.; Ze, H.; Zhang, X.-G.; Zhang, H.; Dong, J.-C.; Shen, T.; Zhang, Y.-J.; Sun, J.-J.; Li, J.-F. In Situ SERS Probing the Effect of Additional Metals on Pt-Based Ternary Alloys toward Improving ORR Performance. *ACS Catal.* **2023**, *13*, 6781−6786.
(144) Begin, E.; Rathnayake, S. T.; Wang, Y.; Schrader, C. M.; Ismail, M. N.; Fox, P.; Wu, S.; Waegele, M. M.; Bao, J. L. Probing the Structure of the Electrochemical Double Layer at a Platinum Electrode Coated with a Metal−Organic Framework. *J. Phys. Chem. C* **2025**, *129*, 2011−2019.
(145) Wang, Y.; Teng, C.; Begin, E.; Bussiere, M.; Bao, J. L. PW-SMD: A Plane-Wave Implicit Solvation Model Based on Electron Density for Surface Chemistry and Crystalline Systems in Aqueous Solution. *J. Chem. Theory Comput.* **2024**, *20*, 6826−6847.
(146) Yang, R.; Wu, M.; Huang, D.; Yang, Y.; Liu, Y.; Zhang, L.; Lai, F.; You, B.; Fang, J.; Liu, T.; Liu, Y.; Zhai, T. Which Dominates Industrial−Current−Density CO_2-to-C_{2+} Electroreduction: $Cu^{\delta+}$ or the Microenvironment? *Energy Environ. Sci.* **2024**, *17*, 2897−2907.
(147) Chen, J.; Wang, L. Effects of the Catalyst Dynamic Changes and Influence of the Reaction Environment on the Performance of Electrochemical CO_2 Reduction. *Adv. Mater.* **2022**, *34*, No. 2103900.
(148) Zheng, Z.; Yao, Y.; Yan, W.; Bu, H.; Huang, J.; Ma, M. Mechanistic Insights into the Abrupt Change of Electrolyte in CO_2 Electroreduction. *ACS Catal.* **2024**, *14* (8), 6328−6338.

(149) Li, L.; Eggert, T.; Reuter, K.; Hörmann, N. G. Electron Spillover into Water Layers: A Quantum Leap in Understanding Capacitance Behavior. *J. Am. Chem. Soc.* **2025**, *147*, 22778−22784.
(150) Li, L.; Reuter, K.; Hörmann, N. G. Deciphering the Capacitance of the Pt(111)/Water Interface: A Micro- to Mesoscopic Investigation by AIMD and Implicit Solvation. *ACS Electrochem.* **2025**, *1*, 186−194.
(151) Heenen, H. H.; Pillai, H. S.; Reuter, K.; Bukas, V. J. Exploring Mesoscopic Mass Transport Effects on Electrocatalytic Selectivity. *Nat. Catal.* **2024**, *7*, 847−854.
(152) Candeago, R.; Wang, H.; Nguyen, M.-T.; Doucet, M.; Glezakou, V.-A.; Browning, J. F.; Su, X. Unraveling the Role of Solvation and Ion Valency on Redox-Mediated Electrosorption through in Situ Neutron Reflectometry and Ab Initio Molecular Dynamics. *JACS Au* **2024**, *4*, 919−929.
(153) Wang, Y.-H.; Zheng, S.; Yang, W.-M.; Zhou, R.-Y.; He, Q.-F.; Radjenovic, P.; Dong, J.-C.; Li, S.; Zheng, J.; Yang, Z.-L.; Attard, G.; Pan, F.; Tian, Z.-Q.; Li, J.-F. In Situ Raman Spectroscopy Reveals the Structure and Dissociation of Interfacial Water. *Nature* **2021**, *600*, 81−85.
(154) Wang, Y.-H.; Li, S.; Zhou, R.-Y.; Zheng, S.; Zhang, Y.-J.; Dong, J.-C.; Yang, Z.-L.; Pan, F.; Tian, Z.-Q.; Li, J.-F. In Situ Electrochemical Raman Spectroscopy and Ab Initio Molecular Dynamics Study of Interfacial Water on a Single-Crystal Surface. *Nat. Protoc.* **2023**, *18*, 883−901.
(155) Peng, X.; Zhu, F.-C.; Jiang, Y.-H.; Sun, J.-J.; Xiao, L.-P.; Zhou, S.; Bustillo, K. C.; Lin, L.-H.; Cheng, J.; Li, J.-F.; Liao, H.-G.; Sun, S.-G.; Zheng, H. Identification of a Quasi-Liquid Phase at Solid−Liquid Interface. *Nat. Commun.* **2022**, *13*, 3601.
(156) Yang, Y.; Qin, J.; Hu, K.; Luo, L.; Kumar, A.; Zhou, D.; Zhuang, Z.; Li, H.; Sun, X. Self-Flooding Behaviors on the Fuel Cell Catalyst Surface: An *in situ* Mechanism Investigation. *Energy Environ. Sci.* **2023**, *16*, 491−501.
(157) Walter, E. D.; Zhang, D.; Chen, Y.; Sung Han, K.; Bazak, J. D.; Burton, S.; O'Harra, K.; Hoyt, D. W.; Bara, J. E.; Malhotra, D.; Allec, S. I.; Glezakou, V.-A.; Heldebrant, D. J.; Rousseau, R. Enhancing CO_2 Transport across a PEEK-Ionene Membrane and Water-Lean Solvent Interface. *ChemSusChem* **2023**, *16*, No. e202300157.
(158) Bisbo, M. K.; Hammer, B. Global Optimization of Atomic Structure Enhanced by Machine Learning. *Phys. Rev. B* **2022**, *105*, No. 245404.
(159) Esterhuizen, J. A.; Goldsmith, B. R.; Linic, S. Interpretable Machine Learning for Knowledge Generation in Heterogeneous Catalysis. *Nat. Catal.* **2022**, *5*, 175−184.
(160) Margraf, J. T.; Jung, H.; Scheurer, C.; Reuter, K. Exploring Catalytic Reaction Networks with Machine Learning. *Nat. Catal.* **2023**, *6*, 112−121.
(161) Spurgeon, S. R.; Ophus, C.; Jones, L.; Petford-Long, A.; Kalinin, S. V.; Olszta, M. J.; Dunin-Borkowski, R. E.; Salmon, N.; Hattar, K.; Yang, W.-C. D.; Sharma, R.; Du, Y.; Chiaramonti, A.; Zheng, H.; Buck, E. C.; Kovarik, L.; Penn, R. L.; Li, D.; Zhang, X.; Murayama, M.; Taheri, M. L. Towards Data-Driven next-Generation Transmission Electron Microscopy. *Nat. Mater.* **2021**, *20*, 274−279.
(162) Ju, Y.; Neumann, O.; Bajomo, M.; Zhao, Y.; Nordlander, P.; Halas, N. J.; Patel, A. Identifying Surface-Enhanced Raman Spectra with a Raman Library Using Machine Learning. *ACS Nano* **2023**, *17*, 21251−21261.
(163) Hu, W.; Ye, S.; Zhang, Y.; Li, T.; Zhang, G.; Luo, Y.; Mukamel, S.; Jiang, J. Machine Learning Protocol for Surface-Enhanced Raman Spectroscopy. *J. Phys. Chem. Lett.* **2019**, *10*, 6026−6031.
(164) Kalinin, S. V.; Mukherjee, D.; Roccapriore, K.; Blaiszik, B. J.; Ghosh, A.; Ziatdinov, M. A.; Al-Najjar, A.; Doty, C.; Akers, S.; Rao, N. S.; Agar, J. C.; Spurgeon, S. R. Machine Learning for Automated Experimentation in Scanning Transmission Electron Microscopy. *npj Comput. Mater.* **2023**, *9*, 227.
(165) Wang, X.; Li, J.; Ha, H. D.; Dahl, J. C.; Ondry, J. C.; Moreno-Hernandez, I.; Head-Gordon, T.; Alivisatos, A. P. AutoDetect-mNP: An Unsupervised Machine Learning Algorithm for Automated Analysis of Transmission Electron Microscope Images of Metal Nanoparticles. *JACS Au* **2021**, *1*, 316−327.
(166) Shen, M.; Li, G.; Wu, D.; Yaguchi, Y.; Haley, J. C.; Field, K. G.; Morgan, D. A Deep Learning Based Automatic Defect Analysis Framework for In-Situ TEM Ion Irradiations. *Comput. Mater. Sci.* **2021**, *197*, No. 110560.
(167) Ziatdinov, M.; Dyck, O.; Maksov, A.; Li, X.; Sang, X.; Xiao, K.; Unocic, R. R.; Vasudevan, R.; Jesse, S.; Kalinin, S. V. Deep Learning of Atomically Resolved Scanning Transmission Electron Microscopy Images: Chemical Identification and Tracking Local Transformations. *ACS Nano* **2017**, *11*, 12742−12752.
(168) Katsuno, H.; Kimura, Y.; Yamazaki, T.; Takigawa, I. Early Detection of Nucleation Events from Solution in LC-TEM by Machine Learning. *Front. Chem.* **2022**, *10*, No. 818230.
(169) Yao, L.; Ou, Z.; Luo, B.; Xu, C.; Chen, Q. Machine Learning to Reveal Nanoparticle Dynamics from Liquid-Phase TEM Videos. *ACS Cent. Sci.* **2020**, *6*, 1421−1430.
(170) Sun, Y.; Zhang, X.; Huang, R.; Yang, D.; Kim, J.; Chen, J.; Ang, E. H.; Li, M.; Li, L.; Song, X. Revealing Microscopic Dynamics: \textitin situ Liquid-Phase TEM for Live Observations of Soft Materials and Quantitative Analysis *via* Deep Learning. *Nanoscale* **2024**, *16*, 2945−2954.
(171) Vuijk, M.; Ducci, G.; Sandoval, L.; Pietsch, M.; Reuter, K.; Lunkenbein, T.; Scheurer, C. Physics-Based Synthetic Data Model for Automated Segmentation in Catalysis Microscopy. *Microsc. Microanal.* **2025**, *31*, No. ozae130.
(172) Timoshenko, J.; Jeon, H. S.; Sinev, I.; Haase, F. T.; Herzog, A.; Roldan Cuenya, B. Linking the Evolution of Catalytic Properties and Structural Changes in Copper−Zinc Nanocatalysts Using \textitoperando EXAFS and Neural-Networks. *Chem. Sci.* **2020**, *11*, 3727−3736.
(173) Martini, A.; Timoshenko, J.; Grosse, P.; Rettenmaier, C.; Hursán, D.; Deplano, G.; Jeon, H. S.; Bergmann, A.; Roldan Cuenya, B. Adsorbate Configurations in Ni Single-Atom Catalysts during CO_2 Electrocatalytic Reduction Unveiled by Operando XAS, XES, and Machine Learning. *Phys. Rev. Lett.* **2024**, *133*, No. 228001.
(174) Martini, A.; Hursán, D.; Timoshenko, J.; Rüscher, M.; Haase, F.; Rettenmaier, C.; Ortega, E.; Etxebarria, A.; Roldan Cuenya, B. Tracking the Evolution of Single-Atom Catalysts for the CO_2 Electrocatalytic Reduction Using Operando X-Ray Absorption Spectroscopy and Machine Learning. *J. Am. Chem. Soc.* **2023**, *145*, 17351−17366.
(175) Liu, Y.; Halder, A.; Seifert, S.; Marcella, N.; Vajda, S.; Frenkel, A. I. Probing Active Sites in Cu_xPd_y Cluster Catalysts by Machine-Learning-Assisted X-Ray Absorption Spectroscopy. *ACS Appl. Mater. Interfaces* **2021**, *13*, 53363−53374.
(176) Wang, X.; Yan, C.; Ondry, J. C.; Bodiwala, V.; Ercius, P.; Alivisatos, A. P. An Artificial Intelligence's Interpretation of Complex High-Resolution in Situ Transmission Electron Microscopy Data. *Matter* **2024**, *7*, 175−190.
(177) Yeh, A. H.-W.; Norn, C.; Kipnis, Y.; Tischer, D.; Pellock, S. J.; Evans, D.; Ma, P.; Lee, G. R.; Zhang, J. Z.; Anishchenko, I.; Coventry, B.; Cao, L.; Dauparas, J.; Halabiya, S.; DeWitt, M.; Carter, L.; Houk, K. N.; Baker, D. De Novo Design of Luciferases Using Deep Learning. *Nature* **2023**, *614*, 774−780.
(178) Hou, K.; Huang, W.; Qi, M.; Tugwell, T. H.; Alturaifi, T. M.; Chen, Y.; Zhang, X.; Lu, L.; Mann, S. I.; Liu, P.; Yang, Y.; De Grado, W. F. De Novo Design of Porphyrin-Containing Proteins as Efficient and Stereoselective Catalysts. *Science* **2025**, *388*, 665−670.
(179) Liu, H.; Song, Z.; Zhang, Y.; Wu, B.; Chen, D.; Zhou, Z.; Zhang, H.-Y.; Li, S.; Feng, X.; Huang, J.; Wang, H. De Novo Design of Self-Assembling Peptides with Antimicrobial Activity Guided by Deep Learning. *Nat. Mater.* **2025**, *24*, 1295−1306.
(180) Chun, H.; Lunger, J. R.; Kang, J. K.; Gómez-Bombarelli, R.; Han, B. Active Learning Accelerated Exploration of Single-Atom Local Environments in Multimetallic Systems for Oxygen Electrocatalysis. *npj Comput. Mater.* **2024**, *10*, 246.

(181) de Jonge, N.; Houben, L.; Dunin-Borkowski, R. E.; Ross, F. M. Resolution and Aberration Correction in Liquid Cell Transmission Electron Microscopy. *Nat. Rev. Mater.* **2019**, *4*, 61−78.

(182) Yang, S.-H.; Choi, W.; Cho, B. W.; Agyapong-Fordjour, F. O.-T.; Park, S.; Yun, S. J.; Kim, H.-J.; Han, Y.-K.; Lee, Y. H.; Kim, K. K.; Kim, Y.-M. Deep Learning-Assisted Quantification of Atomic Dopants and Defects in 2D Materials. *Adv. Sci.* **2021**, *8*, No. 2101099.

(183) Ihara, S.; Saito, H.; Yoshinaga, M.; Avala, L.; Murayama, M. Deep Learning-Based Noise Filtering toward Millisecond Order Imaging by Using Scanning Transmission Electron Microscopy. *Sci. Rep.* **2022**, *12*, 13462.

(184) Vincent, J. L.; Manzorro, R.; Mohan, S.; Tang, B.; Sheth, D. Y.; Simoncelli, E. P.; Matteson, D. S.; Fernandez-Granda, C.; Crozier, P. A. Developing and Evaluating Deep Neural Network-Based Denoising for Nanoparticle TEM Images with Ultra-Low Signal-to-Noise. *Microsc. Microanal.* **2021**, *27*, 1431−1447.

(185) Sadri, A.; Petersen, T. C.; Terzoudis-Lumsden, E. W. C.; Esser, B. D.; Etheridge, J.; Findlay, S. D. Unsupervised Deep Denoising for Four-Dimensional Scanning Transmission Electron Microscopy. *npj Comput. Mater.* **2024**, *10*, 243.

(186) Wang, F.; Henninen, T. R.; Keller, D.; Erni, R. Noise2Atom: Unsupervised Denoising for Scanning Transmission Electron Microscopy Images. *Appl. Microsc.* **2020**, *50*, 23.

(187) Yang, Y.; Feijóo, J.; Figueras-Valls, M.; Chen, C.; Shi, C.; Fonseca Guzman, M. V.; Murhabazi Maombi, Y.; Liu, S.; Jain, P.; Briega-Martos, V.; Peng, Z.; Shan, Y.; Lee, G.; Rebarchik, M.; Xu, L.; Pollock, C. J.; Jin, J.; Soland, N. E.; Wang, C.; Salmeron, M. B.; Chen, Z.; Han, Y.; Mavrikakis, M.; Yang, P. Operando Probing Dynamic Migration of Copper Carbonyl during Electrocatalytic CO_2 Reduction. *Nat. Catal.* **2025**, *8*, 579−594.

https://doi.org/10.1021/acsnano.5c10976
ACS Nano XXXX, XXX, XXX−XXX